Middle Neoproterozoic (Tonian) polar wander of South China: Paleomagnetism and ID-TIMS U-Pb geochronology of the Laoshanya Formation

Justin Tonti-Filippini[1,2], Boris Robert[3,4], Élodie Muller[5,6], André N. Paul[7], Fabian Dellefant[1], Michael Wack[1], Jun Meng[8], Xixi Zhao[9], Urs Schaltegger[7], and Stuart A. Gilder[1]

[1]Dept. of Earth and Environmental Sciences, Ludwig-Maximilians-Universität, Munich, Germany
[2]Centre for Planetary Habitability, University of Oslo, Oslo, Norway
[3]Centre for Earth Evolution and Dynamics, University of Oslo, Oslo, Norway
[4]GeoForschungsZentrum Potsdam, Potsdam, Germany
[5]Université de Paris, Institut de physique du globe de Paris, CNRS, F-75005 Paris, France
[6]IFP Energies Nouvelles, 1-4 Avenue du Bois Préau, 92852 Rueil-Malmaison, France
[7]Dept. of Earth Sciences, Université de Genève, Geneva, Switzerland
[8]School of Earth Sciences and Resources, China University of Geosciences, Beijing, China
[9]IUGS Deep-time Digital Earth program, 88 South Yuhu Road, Kunshan 215300, Jiangsu, China

Key Points:

- High-precision ID-TIMS U-Pb dating yields deposition ages of the Laoshanya Formation (Yangjiaping, South China) between 809 and 804 Ma.
- Discordant paleomagnetic directions in the red beds are a conflation of three temporally distinct field records residing in hematite.
- Our results do not support rapid true polar wander or abnormal magnetic field geometry around 805 Ma.

Corresponding author: Justin Tonti-Filippini, justinto@uio.no

Abstract

Paleomagnetic records of middle Neoproterozoic (820-780 Ma) rocks display high amplitude directional variations that lead to large discrepancies in paleogeographic reconstructions. Hypotheses to explain these data include rapid true polar wander, a geomagnetic field geometry that deviates from a predominantly axial dipole field, a hyper-reversing field (>10 reversals/Ma), and/or undiagnosed remagnetization. To test these hypotheses, we collected 1057 oriented cores over a 85 m stratigraphic succession in the Laoshanya Formation (Yangjiaping, Hunan, China). High precision U-Pb dating of two intercalated tuff layers constrain the age of the sediments between 809 and 804 Ma. Thermal demagnetization isolates three magnetization components residing in hematite which are not time-progressive but conflated throughout the section. All samples possess a north and downward directed component in geographic coordinates at temperatures up to 660°C that is ascribed to a Cretaceous overprint. Two components isolated above 660°C reveal distinct directional clusters: one is interpreted as a depositional remanence, while the other appears to be the result of a mid-Paleozoic (460-420 Ma) remagnetization, which is likely widespread throughout South China. The high-temperature directions are subtly dependent on lithology; microscopic and rock magnetic analyses identify multiple generations of hematite that vary in concentration and distinguish the magnetization components. A comparison with other middle Neoproterozoic paleomagnetic studies in the region indicates that the sudden changes in paleomagnetic directions, used elsewhere to support the rapid true polar wander hypothesis (ca. 805 Ma), are better explained by mixtures of primary and remagnetized components, and/or vertical axis rotations.

Plain Language Summary

Paleomagnetic directions recorded in 820-780 million year old rocks from South China exhibit large amplitude changes that vary rapidly, which have been interpreted to indicate extraordinarily fast motion of Earth's crust and mantle, up to 90° within a five million year span, with respect to the spin axis of the core. This hypothetical phenomenon, called rapid true polar wander, could be responsible for dramatic global environmental change at that time. To test this theory, we collected over 1000 samples from a well exposed section where the incongruous directions are found. Our measurements suggest that some of the rocks acquired a new magnetic signal during a pervasive remagnetization event in South China around 440 million years ago, long after original deposition of the rocks. New hematite growth has a demagnetization spectrum that partially overlaps or completely obscures the original magnetic signal, which was previously unrecognized. This implies that rapid true polar wander is likely an artefact of magnetic overprinting in ancient rocks from South China. Our results suggest that South China was in a relatively stable position at high latitudes 809-804 million years ago. We find no evidence to support exceptionally fast continental drift or an abnormal geomagnetic field geometry during that time.

1 Introduction

Magnetic directions preserved in rocks and sediments can be used to estimate past positions of the geomagnetic pole, known as virtual geomagnetic poles (VGPs). A sequence of rocks spanning several million years in time may record progressive changes in VGP position, which can be used to construct an apparent polar wander path (APWP). APWPs represent the combined effect of tectonic plate motion and the net rotation of the mantle and crust with respect to Earth's rotational pole, called true polar wander (Evans, 2003). A key assumption is that Earth's magnetic pole aligns with the geographic (spin) axis, which is known as the geocentric axial dipole (GAD) hypothesis. If the GAD hypothesis is valid, then APWPs can be used to determine past locations of tectonic

plates and reconstruct cycles of continental assembly and breakup; globally correlated APWPs can be used to estimate rates of true polar wander.

A key challenge in paleomagnetism is to build accurate APWPs back into the Precambrian (Kodama, 2013). Of particular interest is the Neoproterozoic Era, which saw the end of prolonged environmental stability between 1.8 – 0.8 Ga, a period referred to as the Boring Billion (N. M. Roberts, 2013), as well as intermittent episodes of Snowball Earth and extreme greenhouse conditions (Hoffman et al., 1998), culminating in the Cambrian explosion and diversification of complex life after ca. 539 Ma (Cohen et al., 2013, version 2023/04). An explanation of Earth's paleogeography and unique climatic behaviour in the Neoproterozoic is crucial for discerning drivers of long-term climate change and biological evolution. Central to this challenge is unravelling the assembly of the Rodinia supercontinent prior to ca. 900 Ma and its break-up after ca. 750 Ma (Z. X. Li et al., 2008), but Rodinia's configuration is still debated. Torsvik (2003) described Rodinia as 'a jigsaw puzzle where we must contend with missing and faulty pieces and have misplaced the picture on the box'. The South China Block (SCB) constitutes one of the most enigmatic puzzle pieces, whose Neoproterozoic history has plagued efforts to build a cohesive model of Rodinia (Evans et al., 2016; Cawood et al., 2020; Jing et al., 2021; Park et al., 2021).

Resolving the position and orientation of the SCB in the Neoproterozoic, particularly around 820 – 800 Ma, is complicated by the hypothesized occurrence of one or two rapid true polar wander (TPW) events which may have rotated Earth's mantle and lithosphere 55 – 90° with respect to the spin axis (e.g., Z. X. Li et al., 2004; Niu et al., 2016; Jing et al., 2020). Large-scale oscillating TPW events (e.g., Fig. 1a), known as inertial interchange true polar wander (IITPW), have been postulated to resolve discordant paleomagnetic directions from other continents and are linked to dramatic global environmental change observed around the same time (Kirschvink et al., 1997). Sudden directional changes observed in South China have been compared with paleomagnetic observations from Svalbard (Maloof et al., 2006), and speculatively correlated with the onset of a global negative carbon isotope anomaly, the Bitter Springs Stage, known as the Bitter Springs TPW hypothesis (Swanson-Hysell et al., 2012).

The debate over South China's position in Rodinia is convolved with the Bitter Springs TPW hypothesis, as paleomagnetic data from the SCB undergo rapid paleolatitude variations between 820 and 780 Ma. Various reconstructions of Rodinia place the SCB in a central, marginal or completely isolated position (Fig. 1b). Classic 'missing link' models place the SCB at a low latitude between Laurentia and Australia (e.g., Z. X. Li et al., 2008), while other models such as SWEAT (Southwest US – East Antarctica) place the SCB adjacent to India and/or NW Australia, allowing for a direct fit between Australia and Laurentia (Yao et al., 2019). It is also possible that South China was entirely disconnected from Rodinia and occupied a position near the north pole (e.g., Park et al., 2021). Increasingly, models appear to challenge a SWEAT configuration in the Neoproterozoic, although more and more studies suggest that Australia, India and South China were geographically close through the late Cryogenian to Ediacaran (S. Zhang et al., 2021, and references therein).

Maloof et al. (2006) and Swanson-Hysell et al. (2012) suggested that testing of the Bitter Springs TPW hypothesis necessitates robust paleomagnetic and geochronologic studies of continuous sedimentary sequences from several cratons. If the rapid TPW hypothesis is valid, then all strata that span the Bitter Springs Stage [ca. 810 – 800 Ma Halverson et al. (2022)], should show similar excursions in their isotopic and paleomagnetic signals. Resolving these discordant paleomagnetic directions, currently observed only in Svalbard and South China, calls for integrative studies and is an issue of 'major geodynamic significance' (Evans et al., 2016). Raub et al. (2015) notes that the TPW events hypothesized by Maloof et al. (2006) are not directly dated so cannot be precisely correlated with data from South China. This allows for considerable flexibility in

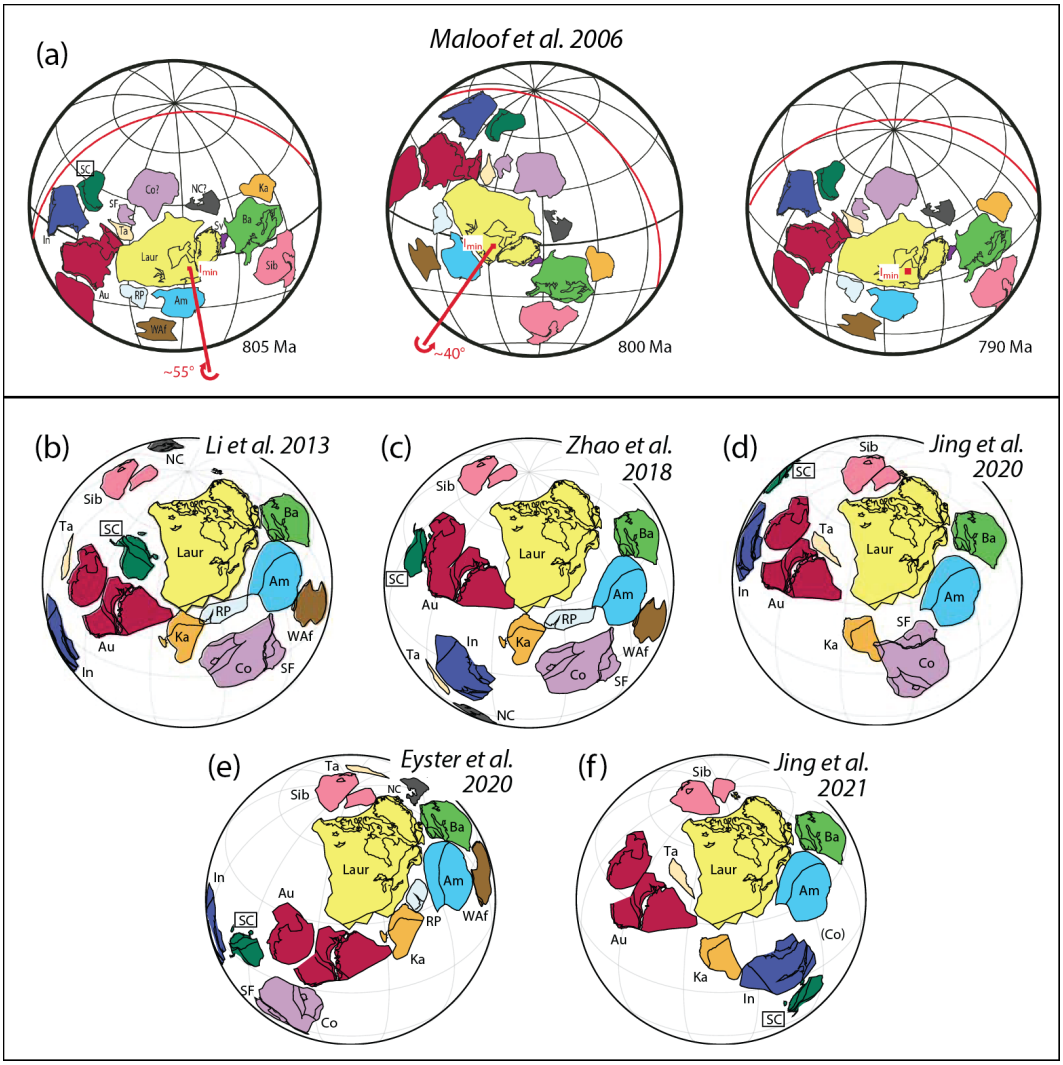

Figure 1. (a) Paleogeographic reconstructions of Rodinia during a hypothesized rapid true polar wander (TPW) event between 805 and 790 Ma; the TPW rotation axis (I_{min}) is marked in red (after Maloof et al., 2006). (b-f) Proposed reconstructions of Rodinia with Laurentia fixed in present North American coordinates, modified from Evans (2021). South China occupies completely different positions in each reconstruction (see Z. X. Li et al., 2013; Zhao et al., 2018; Jing et al., 2020; Eyster et al., 2020; Jing et al., 2021). Am = Amazonia, Au = Australian cratons including Mawsonland, Ba = Baltica, Co = Congo, In = India, Ka = Kalahari, Laur = Laurentia, NC = North China, RP = Rio Plata, SC = South China, SF = Sao Francisco, Sib = Siberia, Sv = Svalbard, Ta = Tarim, WAf = West Africa.

paleogeographic models around 800 Ma, so the TPW hypothesis and the precise configuration of Rodinia 'must await better constraints' (Raub et al., 2015).

Other plausible explanations for South China's discordant paleomagnetic data include rapid tectonic plate motion or non-dipolar to hyper-reversing geomagnetic fields driven by nucleation of Earth's inner core (e.g., Driscoll, 2016). Peculiar APWPs could also be an artefact of undiagnosed remagnetization. For example, Q. R. Zhang and Piper (1997) warned that South China experienced several episodes of tectonic reworking and suffered extensive sub-tropical weathering, thereby highlighting challenges to paleomagnetism, especially going far back in time. Indeed, numerous studies from South China are based on red sedimentary rocks that have complicated magnetization histories; hence, caution is required when interpreting paleomagnetic signals in red beds.

The Yangjiaping (Hunan Province, China) area has a fairly complete geologic record from the Neoproterozoic through the Paleozoic, including Marinoan tillites and cap carbonates (Macouin et al., 2004). Below the tillites lie the Laoshanya Formation red beds, which were previously dated at Yangjiaping to 809 ± 16 Ma (Yin et al., 2003). There, we collected 1057 paleomagnetic cores in a 85 metre-thick section, freshly exposed along a river, as well as 14 cores in the underlying Lengjiaxi Group. We present a paleomagnetic study of those samples, combined with rock magnetic, mineralogical and microscopic analyses, as well as ID-TIMS U-Pb zircon geochronology of intercalated tuffs, in order to shed light on Neoproterozoic geomagnetic field behaviour and the paleogeography of South China around 820 – 800 Ma.

2 Geological setting

2.1 Nanhua rift basin

The South China Block (SCB) consists of two major tectonic elements, the Yangtze craton to the northwest and the Cathaysia block to the southeast (Fig. 2a). The SCB assembled between 1000 – 820 Ma in a series of suprasubduction zone arc-backarc systems and accretionary orogenesis (Cawood et al., 2013), with final assembly/suturing completed ca. 830 - 816 Ma (Park et al., 2021), an event referred to as the Jiangnan or Sibao orogeny. There is still controversy over the timing of their amalgamation, but it is generally accepted that the two blocks formed the SCB when they collided along the Jiangshan-Shaoxing suture zone (J. Wang et al., 2015, and references therein). After ∼820 Ma, during the hypothesized breakup of Rodinia, the Nanhua rift basin developed along the suture zone (S. Zhang et al., 2008), which accumulated sediments through the Neoproterozoic to early Paleozoic (Charvet, 2013). Several rifting phases likely occurred in the basin as indicated by bimodal magmatism ca. 830 – 820 Ma; the lower sequences are dominated by volcaniclastic sedimentary rocks that are interpreted to be continental rift deposits (J. Wang & Li, 2003).

Rifting terminated in the Nanhua basin in the late Ordovician to early Silurian (460 – 400 Ma), perhaps due to inversion of the basin in response to continental convergence (Xu et al., 2016), an enigmatic episode known by several names including the Caledonian (Y. Wang et al., 2007), Wuyi-Yunkai (Z. X. Li et al., 2010) and Kwangsian (Zheng et al., 2020) orogenic event. We refer to this episode as the Wuyi-Yunkai Orogeny. An explanation for the geodynamic processes that triggered the Wuyi-Yunkai Orogeny is a persistent problem, although an angular unconformity between South China's pre-Devonian and Devonian strata is widespread (Charvet, 2013). Mid-Paleozoic metamorphic and magmatic rocks, as well as evidence of folding and thrusting, are found throughout the Jiangnan orogen and Cathaysia block, but the tectonic response to the Wuyi-Yunkai Orogeny is not well understood within the Yangtze craton (Zheng et al., 2020).

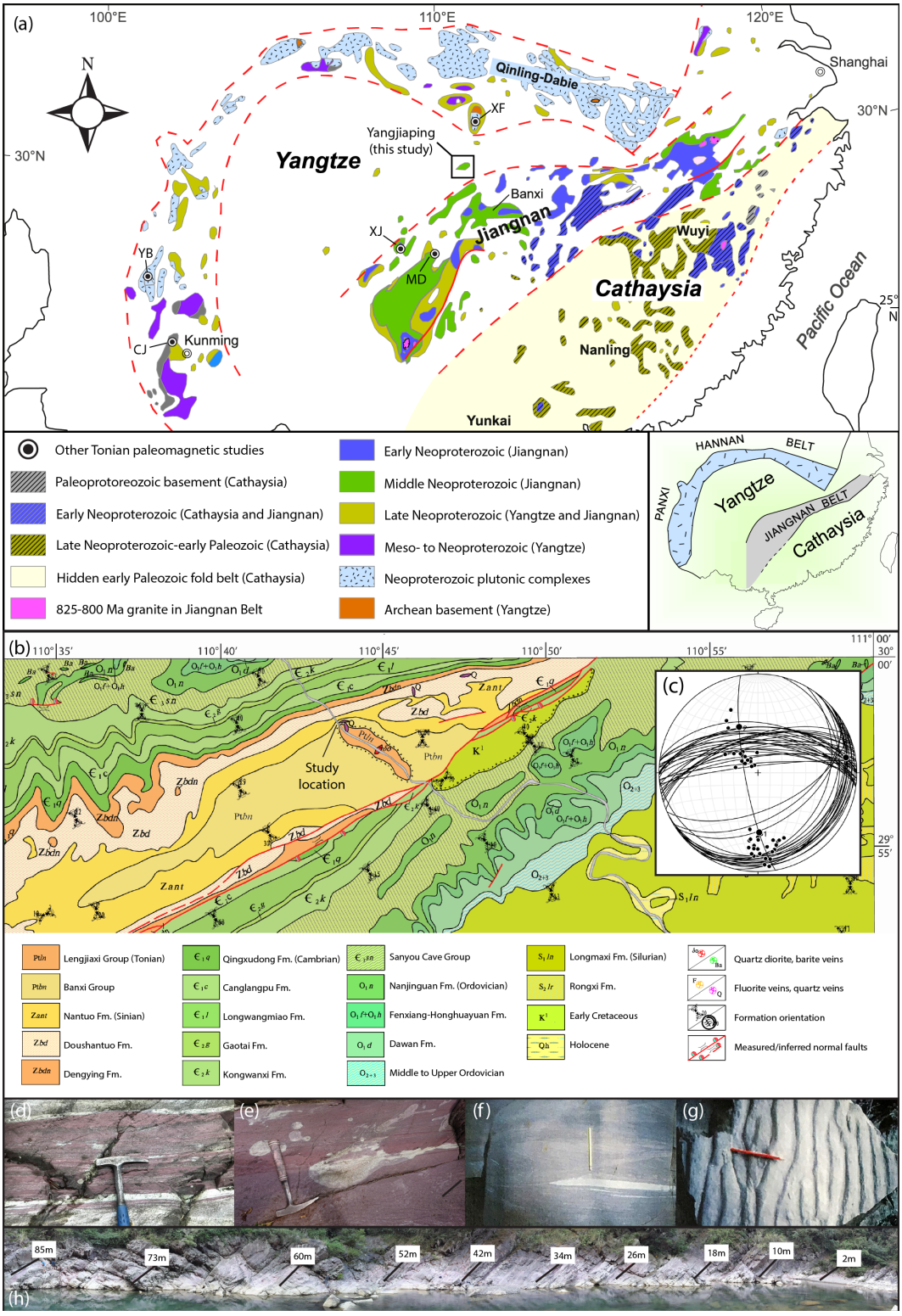

Figure 2. (a) Simplified regional map highlighting the Neoproterozoic in South China (after Cawood et al., 2018). Table S1 lists the Tonian studies (black circles with initials). (b) Geological map of the Yangjiaping area, northwest Hunan (after C. Li et al., 2017). (c) Measured bedding strikes and dips in the area indicates near-cylindrical folding, with a slightly plunging (11°) axis trending 80°. (d-g) Field photos of the Laoshanya Formation showing (d) alternating green-grey and purple-red sandstones, (e) leaching of the red beds (whitish color) that cuts across bedding, (f) cross-bedding, and (g) ripple marks. (h) Composite photo of sampled section with stratigraphic heights.

2.2 Banxi group

One of the key rifting successions in the Nanhua basin is the Banxi Group siliclastic sequence (ca. 820 – 730 Ma) that crops out towards the south-eastern edge of the Yangtze craton and is widely exposed in Hunan Province (S. Zhang et al., 2008). The Banxi Group is thought to have formed in an intra-continental rift environment and is characterized by thick sedimentary successions and bi-modal magmatism (Cawood et al., 2018). The Banxi Group in Hunan Province has been considered equivalent to the Danzhou Group in northern Guangxi Province (H. Zhang, 1998) and the Xiajiang Group in eastern Guizhou Province (Lan et al., 2015; Park et al., 2021); however, the age of the base of the Danzhou Group is poorly constrained (Song et al., 2017).

Around the study area, the Banxi Group overlies the Lengjiaxi Group with an angular unconformity (the Wuling unconformity), which crops out throughout the orogen and is broadly constrained as 830 – 813 Ma (D. Li et al., 2022). In north-central Hunan, the Cangshuipu Group volcanics were emplaced between the Banxi and Lengjiaxi groups. These volcanics were dated at 824 – 814 Ma (J. Wang et al., 2003; Y. Zhang et al., 2015), which provide an additional constraint on the lower age of the Banxi Group. The Banxi Group consists of the Madiyi Formation in the lower part and the Wuqiangxi in the upper (S. Zhang et al., 2008). The Xihuangshan disconformity (800 – 779 Ma) separates the Madiyi and Wuqiangxi Formations (D. Li et al., 2022), referred to elsewhere as the Zhangjiawan and Xieshuihe Formations, respectively (J. Wang et al., 2003).

The Madiyi Formation crops out across Hunan and is thought to have formed in a shallow marine, oxidizing environment. In northwest Hunan, the formation comprises alternating sequences of distinct dark purple-red mudstones and green sandstones (Fig. 2h). A regional study of detrital zircons in the Madiyi Formation yielded age peaks (lower limits) at ~ 808 Ma in the lowermost part, and $803 - 800$ Ma in the uppermost part (D. Li et al., 2022). The Madiyi Formation is characterized as relatively Fe_2O_3-rich and may act as a geochemical barrier in the region: $\sim 80\%$ of the gold deposits in northwest Hunan are hosted in the Madiyi Formation (S. X. Yang & Blum, 1999). The Laoshanya Formation is synonymous with the Madiyi Formation in Yangjiaping (Yin et al., 2003), although recent work suggested the Madiyi Formation may be slightly younger (Y. Zhang et al., 2015; Xian et al., 2020; Park et al., 2021). We use Laoshanya to refer specifically to the outcrop in Yangjiaping, and Madiyi to refer to the wider formation, as our dating shows them to be the same age (Section 4.1).

2.3 Yangjiaping section

The Yangjiaping section lies in the northwestern Nanhua rift basin (Fig. 2b) (X. Zhang et al., 2000; Song et al., 2017). Yangjiaping is an important landmark for the Precambrian geology of South China and was selected as a 'candidate stratotype section' for the Nanhua system (Yin et al., 2003). At Yangjiaping, the Laoshanya Formation is 148 metres thick (Yin et al., 2004) and presents a continuous sequence of alternating purple-red and green-grey sandstones and siltstones (Fig. 2d). For comparison, Madiyi in the southeast part of the basin may be 3500 metres thick (S. Zhang et al., 2008). The Laoshanya Formation is well-preserved and shows evidence of a shallow marine, near-shore or tidal environment, with cross-bedding (Fig. 2f) and ripple marks (Fig. 2g). Some beds contain sub-vertical quartz and calcite veinlets up to several centimetres wide. White to pale green 'mottling' is ubiquitous (Fig. 2e), often cross-cutting the purple beds, which is evidence of localized leaching of iron by secondary fluids (Parry et al., 2004).

The Laoshanya Formation is conformably overlain by the Xiushuihe (Wuqiangxi) Formation (Fig. 3), dated at 758 ± 23 Ma by the Sensitive High Resolution Ion Microprobe (SHRIMP) method (Yin et al., 2003). Twelve metres below the Xiushuihe/Laoshanya contact lies a tuff whose SHRIMP zircon U-Pb date constrained the upper age of the Laoshanya Formation to 809 ± 16 Ma (Yin et al., 2003). The Laoshanya

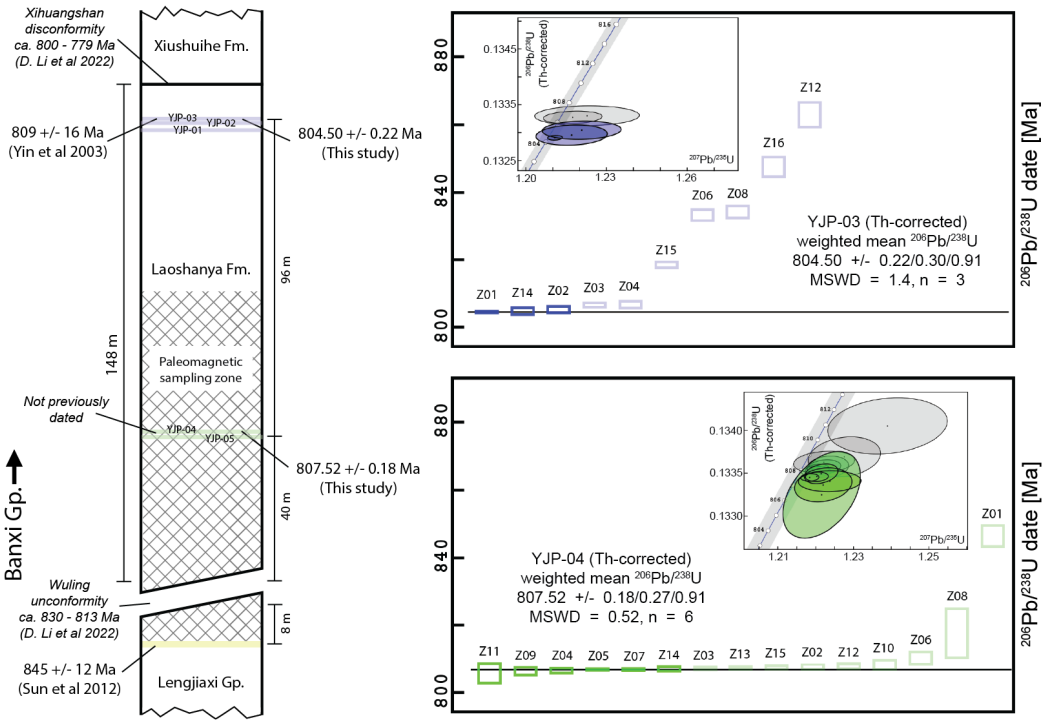

Figure 3. Geochronology of the Laoshanya Formation in Yangjiaping with locations of interbedded tuffs (blue, green and yellow stripes). A five metre thick conglomerate marks the base of our section, below which 14 cores were sampled in the Lengjiaxi Group. Previously published dates are shown on the left side of the column; our new dates (YJP-03 and YJP-04) are shown on the right. Coloured rectangles indicate Th-corrected $^{206}Pb/^{238}U$ dates for individual zircons with 2σ analytical uncertainty; transparent rectangles indicate results excluded from weighted means. Corresponding $^{206}Pb/^{238}U$ – $^{207}Pb/^{235}U$ concordia diagrams are inset.

Formation (strike/dip = 255°/58°) uncomformably overlies the Lengjiaxi Group (258°/87°), dated elsewhere at 860 – 835 Ma (Y. Zhang et al., 2015). A five metre thick conglomerate distinguishes the unconformity, which demarcates the base of our section. SHRIMP U-Pb dating of laminated tuff from the underlying Lengjiaxi Group in Yangjiaping yielded 845 ± 12 Ma (Sun et al., 2012).

The Doushantuo Formation (599 ± 4 Ma) in Yangjiaping yielded a single-polarity magnetization that passed a fold test and was interpreted to be primary, indicating a low-latitude position for South China in the Ediacaran (Macouin et al., 2004). However, S. Zhang et al. (2015) remarked that the formation does not contain the pattern of reversals common for the Ediacaran elsewhere; the paleopole lies close to other early Cambrian and Silurian poles for South China; and the positive fold test implies only that the magnetization is pre-folding and not necessarily primary. Macouin et al. (2004) recognized the similarity of their pole to early Silurian poles, although they considered the loop in South China's APWP between the Ediacaran and Silurian to be a robust feature and not an artefact of remagnetization. More detailed rock magnetic data suggested an episode of magnetite dissolution during early diagenesis (Macouin et al., 2012).

South China was shaped by large-scale Mesozoic deformation in response to the collision of the North and South China blocks that ended by the late Jurassic (Gilder & Courtillot, 1997; Yan et al., 2003). This collision likely produced the folding at Yangjiaping seen in

Fig. 2(b) (Gilder et al., 1999). J. Yang et al. (2021) identified angular unconformities between Middle Triassic and Jurassic strata, and between Cretaceous and pre-Cretaceous strata 20 – 40 km south of Yangjiaping. At Yangjiaping, the Laoshanya Formation through the late Ordovician Wufeng Formation [442 ± 8 Ma (Xie et al., 2012)] have consistent strikes $250 - 280°$ and dips $55 - 70°$, suggesting a lack of significant deformation until at least the end of the Ordovician. Similarly, no angular unconformity exists between the Neoproterozoic Danzhou Group and Ordovician sedimentary rocks in northern Guangxi, ∼500 km to the south (S. Li et al., 2022).

3 Methods and equipment

3.1 Sampling campaigns

We collected paleomagnetic samples in September 2019 along a river at Yangjiaping (Fig. 2b) (Shimen County, Hunan Province) opposite the J01 County Road (29.970°E, 110.732°N). 1057 oriented cores, 2.5 cm in diameter, were drilled over a stratigraphic thickness of 85 m starting at the base of the Laoshanya Formation (Fig. 3), with a nominal spacing of 5-10 cm; occasionally we drilled 4 or 5 cores in the same horizon with each sample separated along strike by 10's to 100's of cm. An additional 14 cores were drilled over a stratigraphic thickness of 5 m at the top of the underlying Lengjiaxi Group (below the conglomerate). All cores were oriented with sun (when possible) and magnetic compasses. The median magnetic anomaly from the sun compass was -3.4 ± 0.6° (n = 269), indistinguishable from that expected (-3.7°) from the IGRF2020 model (Alken et al., 2021) at Yangjiaping; all compass azimuths were corrected accordingly. In August 2021, five ∼2 kg samples were collected from suspected volcanic tuff horizons within the Yangjiaping section for U-Pb dating (Fig. 3).

3.2 U-Pb geochronology

High precision U-Pb zircon dating was performed using chemical abrasion - isotope dilution - thermal ionization mass spectrometry (CA-ID-TIMS) at the University of Geneva. Mineral separation involved crushing and milling bulk samples to <300 µm, followed by concentration on a Wilfley table, Frantz magnetic separator and heavy liquids (methylene iodide, density 3.32 g/ml). Crack and inclusion-free zircon crystals were hand-picked under a binocular microscope, thermally annealed at 900°C for 48 hours, and then partially dissolved in concentrated hydrofluoric acid (HF) at 210°C for 12 hours in a Parr^{TM} bomb vessel (Widmann et al., 2019). The partially dissolved grains were then extracted and washed in 6N HCl in 3 ml Savillex beakers overnight (min. 12 h) at 80°C. Individual zircons were washed 4x with 7N HNO_3 in 3 ml Savillex beakers placed in an ultrasonic bath. Samples were then transferred into 200 µl Savillex microcapsules, mixed with 1-2 drops of EARTHTIME ^{202}Pb-^{205}Pb-^{233}U-^{235}U (ET2535) tracer solution (Condon et al., 2015; McLean et al., 2015) and dissolved with 2-3 drops of concentrated HF in Parr^{TM} digestion vessels at 210°C for 48 hours. After dissolution, samples were dried at 120°C, re-dissolved in 3N HCl, and then U and Pb were separated using anion exchange column chemistry. Chemical preparation was carried out in a class 100 clean-air facility. U and Pb were loaded together on outgassed, zone-refined, Re filaments with a silica-gel/phosphoric acid emitter solution (Gerstenberger & Haase, 1997), and measured on either a Thermo Scientific Triton TIMS or an IsotopX Phoenix TIMS.

The measured isotopic ratios were corrected for interferences of $^{238}U^{18}O^{16}O$ on $^{235}U^{16}O_2$ using a $^{18}O/^{16}O$ composition of 0.00205 based on repeat measurements of the U500 standard. Mass fractionation of U was corrected using a double isotope tracer with a $^{235}U/^{233}U$ of 0.99506 ± 0.00005 (1σ). The Pb blank isotopic composition is $^{206}Pb/^{204}Pb$ = 17.84 ± 0.37 (1σ), $^{207}Pb/^{204}Pb$ = 15.25 ± 0.33 (1σ) and $^{208}Pb/^{204}Pb$ = 37.05 ± 0.90 (1σ), based on total procedural blank measurements. Repeat analyses of the ET100 solution ($^{206}Pb/^{238}U$ date: 100.173 ± 0.003 Ma; Schaltegger et al., 2021) yielded a value

of 100.1678 ± 0.0046 Ma (MSWD = 3.2, n = 32/40). All zircon $^{206}Pb/^{238}U$ dates were corrected for ^{230}Th-^{238}U disequilibrium using a Th/U_{magma} of 3.5 ± 1.0.

To determine the U-Pb age of each tuff, we take the youngest cluster of ≥ 3 analyses, assuming the zircons crystallised until the time of eruption and all Pb-loss is mitigated by the chemical abrasion procedure, in line with previous U-Pb ID-TIMS studies which show that youngest date clusters are generally a reliable measure for eruption age (e.g., Schaltegger et al., 2015; Edward et al., 2023). Older dates are assumed to be from recycled zircons or associated with inherited cores, wall rock contamination, and/or prolonged growth in magma chambers. We report weighted mean U-Pb age uncertainties at the 2σ level in the format A±X/Y/Z, where A = weighted mean age, X = analytical uncertainty, Y = combined analytical and tracer uncertainty, and Z = combined analytical, tracer and decay constant uncertainty (Schoene et al., 2006).

3.3 Paleomagnetism

Paleomagnetic samples were measured at the Paleomagnetic Laboratory, Ludwig-Maximilians-Universität (LMU-Munich). Cores were cut into 2.2 cm high cylindrical specimens using a non-magnetic saw. Specimens were thermally demagnetized in a magnetically-shielded, paleomagnetic oven with an accuracy of ± 1°C (Volk, 2016). Remanent magnetizations were measured using a 2G Enterprises superconducting rock magnetometer via the automated SushiBar system (Wack & Gilder, 2012). Before treatment and after each heating step, bulk susceptibilities were measured at room temperature with a Bartington MS2 susceptibility meter. Repeat measurements on a subset of specimens were measured with an Agico JR6 spinner magnetometer to check for consistency. 22 specimens underwent stepwise alternating field (AF) demagnetization up to 90 mT prior to thermal demagnetization, which generally removed <10% of the natural remanent magnetization (NRM) so was discontinued. All paleomagnetic measurements were made inside a 90 m^3 magnetically shielded room with an average residual field <500 nT.

3.4 Rock magnetism

Based on the paleomagnetic experiments, select samples were subjected to a suite of rock magnetic investigations. Samples were crushed into powder using a porcelain mortar (unsieved). Hysteresis parameters and isothermal remanent magnetization (IRM) acquisition curves in applied fields up to 1.8 T were measured with a Princeton Measurements Corporation MicroMag 3900 vibrating sample magnetometer (VSM) at LMU-Munich. Low temperature experiments were performed on the same instrument down to 77 K with a liquid nitrogen cryostat. Thermal susceptibility curves were measured up to 700°C in air using a Agico MFK1-FA Kappabridge with a CS-4 furnace at the University of Oslo. Anisotropy of magnetic susceptibility (AMS) measurements on 99 non-demagnetized core specimens were carried out with an Agico MFK1-FA Kappabridge at the University of Tübingen, with a peak field intensity of 200 A/m and an operating frequency of 976 Hz. Anisotropy of anhysteretic magnetic remanence (AMR) measurements were made on the same 99 specimens using the SushiBar at LMU-Munich with a peak AF field of 90 mT and a DC bias field of 0.1 mT (Wack & Gilder, 2012).

3.5 Mineralogical and microscopic analyses

25 samples were selected for mineralogical analyses. Polished thin sections were first observed using transmitted and reflected light microscopy at LMU-Munich. Scanning electron microscopy (SEM) analyses were performed with a Hitachi SU5000 Schottky Field-Emission Gun (FEG) SEM (LMU-Munich), and on core slices polished to 0.5 µm with a Zeiss Ultra55 FEG SEM at the Institut de Minéralogie, Physique des Matériaux et de Cosmochimie (Paris). Backscattered secondary electron (BSE) images were acquired

using an angle selective backscattered detector with accelerating voltages of 15 - 20 kV, and working distances of 7.5 - 10 mm. Elemental compositions were determined by energy dispersive X-ray spectrometry (EDXS) using an QUANTAX EDS detector after copper calibration. Semi-quantification of the spectra was achieved using the ESPRIT software package (Bruker) and the phi-rho-z method.

Results from EDXS elemental composition data obtained by SEM were cross-checked with XRD measurements to more confidently identify the mineralogy. Four ∼10 g core samples were finely ground and homogenized in an agate mortar for X-ray diffraction (XRD) at the Institut de physique du globe de Paris (IPGP, France). XRD analyses on the powders were performed using a Panalytical Xpert Pro transmission diffractometer with a copper anode operated at 45 kV and 40 mA and a slit of 0.5° at a 240 mm radius. The 2θ scan was performed in continuous mode from 4° to 90° (2θ) with steps of 0.0001°. Peak identification was performed using pattern search on the X-ray diffraction database of reference spectra Crystallography Open Database (`http://www.crystallography.net`).

4 Results and observations

4.1 U-Pb geochronology

Samples YJP-01, YJP-02 and YJP-03 lie 12 m below the top of the Laoshanya Formation (Fig. 3); YJP-01 and YJP-03 are 1.8 m apart. Samples YJP-04 and YJP-05 (0.6 m apart) lie 40 m above the base of the formation, near the middle of the paleomagnetic sampling zone, 96 m below YJP-01. Song et al. (2017) measured a stratigraphic thickness of 184 m for the Laoshanya Formation in Yangjiaping (perhaps along the road); our measurements on the riverside outcrop match the stratigraphic thickness of 148 m obtained by Yin et al. (2004).

Analyses of 44 individual zircons from the upper three samples (YJP-01 to YJP-03) yielded dates predominantly between 863 and 804 Ma based on Th-corrected $^{206}Pb/^{238}U$ ratios, with minor (n<4) clusters at 1.0, 1.7, 2.0 and 2.4 Ga. Sample YJP-03 yielded the youngest age plateau at 804.50 ± 0.22/0.30/0.91 Ma (MSWD = 1.4, n = 3), which we interpret as the depositional age for this part of the section. YJP-01 and YJP-02 contained many subhedral or rounded zircons that yielded dates between 861 and 807 Ma, with no distinct plateau, which we interpret as inherited or recycled.

We analyzed 29 zircons from the lower sample group. Sample YJP-04 contained hundreds of pristine euhedral zircons and yielded the youngest age plateau at 807.52 ± 0.18/0.27/0.91 Ma (MSWD = 0.52, n = 6), which is interpreted as the depositional age. YJP-05 contained large subhedral zircons that yielded scattered dates between 1015 and 818 Ma, with an age plateau at 818.91 ± 0.18/0.27/0.92 Ma (MSWD = 0.45, n = 3). Given that YJP-05 is situated only 0.6 m below YJP-04, we consider it unlikely that this is a true depositional age as it implies a hiatus of 11.4 Myr which is not supported by field observations. Th/U_{zircon} ratios for YJP-05 are also lower (<0.75) than those of YJP-03 and YJP-04 (generally 0.9 to 1.2), suggesting a different provenance or metamorphic overgrowth, and increased likelihood of inheritance. Moreover, a depositional age >814 Ma would be superpositionally inconsistent with the inferred ages of the underlying Wuling unconformity and the Cangshuipu volcanics.

Assuming no significant depositional hiatuses exist, these results yield an accumulation rate of 32 ± 4 m/Myr (or 3.2 ± 0.4 cm/kyr) for the Laoshanya Formation (with analytical uncertainty only). Using linear extrapolation (Blaauw & Christeny, 2011), our findings suggest that the Laoshanya Formation was deposited between 808.7 [median, 95% range = 809.6-808.0] and 804.2 [median, 95% range = 804.7-803.5] Ma (Fig. S4), and can be broadly correlated with the lower Madiyi Formation and upper Xiajiang Group. Our results agree well with the regional compilation of D. Li et al. (2022) who reported age peaks in detrital zircons at ∼ 808 Ma for lower Madiyi and 803 to 800 Ma for upper

Table 1. Summary of paleomagnetic results from Yangjiaping (29.970°N, 110.732°E). n = number of specimens. D and I are declination and inclination in (g) geographic (in situ) and (s) stratigraphic (tilt-corrected) coordinates (°). κ and α_{95} are the precision parameter and 95% confidence ellipse (Fisher, 1953). Pos./neg. rev. test = positive or negative reversal test after McFadden and McElhinny (1990). A, B and C refer to the magnetization component.

Name	n	D_g	I_g	D_s	I_s	κ	α_{95}	Comments
Lengjiaxi Gp.								Strike/dip = 258/87
Lengjiaxi A	14	24.6	58.3	7.8	-22.2	269.3	2.4	Neg. fold test
Laoshanya Fm.								Strike/dip = 255/58
Laoshanya A	1002	24.5	55.9	5.9	4.1	29.3	0.8	Neg. fold test
Laoshanya B	100	33.8	-61.9	133.8	-46.9	15.8	3.7	
Laoshanya C	81	149.4	42.5	30.3	73.8	33.6	2.8	Neg. rev. test
Laoshanya C*	44	150.9	43.4	25.4	74.1	48.3	3.1	Pos. 'B' rev. test

*Filtered for specimens that decay linearly to the origin and have MAD $< 10°$ (Fig. S3).

Madiyi. The age of 807.52 ± 0.18/0.27/0.91 Ma in the middle (40 m height) of the paleomagnetic sampling zone is assigned to the paleopole in the following sections.

4.2 Paleomagnetic results

1188 specimens were thermally demagnetized up to 680°C with progressive decreases in temperature steps from 100 to 2°C (Fig. 4). Many specimens demonstrated erratic demagnetization behaviour above 660°C which was accompanied by a large (tenfold) increase in bulk susceptibility, indicating alteration. Three coherent components (A, B and C) were identified using principal component analysis (Kirschvink, 1980), as described below and shown in Fig. 4 with summaries in Fig. 5 and Table 1. Specimens often appeared to contain variable concentrations of all three components, which could be resolved and quantified with vector unmixing analyses (Tonti-Filippini & Gilder, 2023). Some samples also contained a spurious component which demagnetized below 100-200°C and generally aligned with the present day field; this is interpreted to be a viscous remanent magnetization (see Butler, 1992, Chapter 3) and not considered further.

4.2.1 Components A, B and C

1016 specimens (86%) contained a coherent north and down (in situ coordinates) directed component that unblocked mostly between 100 and 660°C (Figs. 4a and d). This component is referred to as component A and is ubiquitously present in both the Laoshanya Formation (n = 1002) and the Lengjiaxi Group (n = 14). Component A often occurs in combination with a higher temperature component (B or C), although in ca. 6% of the specimens, it is the sole magnetization component. A fold test is negative at 99% confidence limits (McElhinny, 1964), indicating component A was acquired after folding.

181 specimens (15%) displayed coherent demagnetization behaviour from 660 to 680°C that decays to the origin on Zijderveld diagrams (Fig. 4b and c). The high-temperature directions form two clusters on a stereonet (Figs. 5b and c), which are referred to as components B (n = 100) and C (n = 81). Component B consists of single-polarity, southeast and up directions in tilt-corrected (stratigraphic, s) coordinates (Fig. 5b). Despite spanning 85 metres of section, component B directions are present only in one polarity.

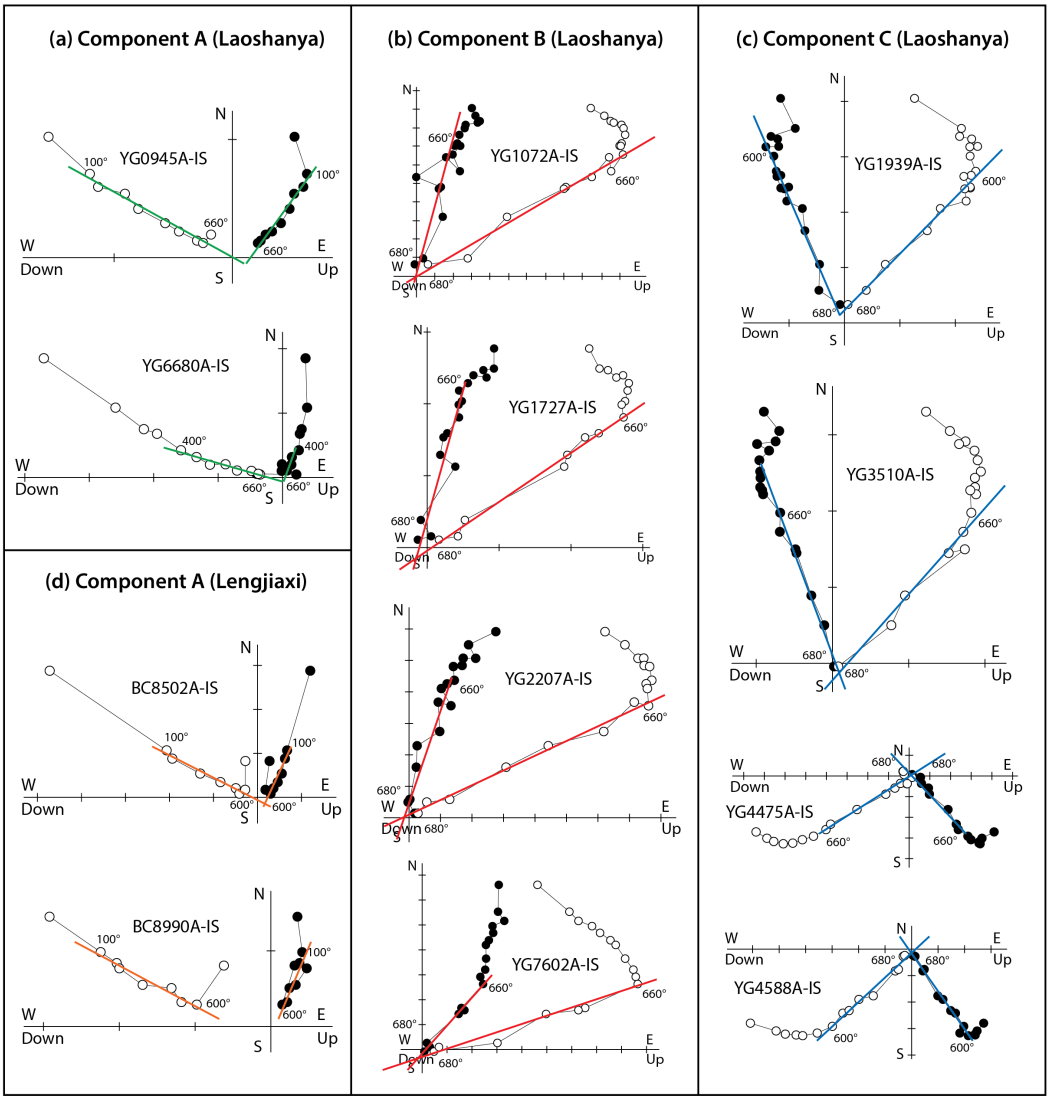

Figure 4. Zijderveld (1967) diagrams of representative samples (in geographic coordinates) from the three component groups (A-C) from the Yangjiaping section displayed with best-fitting ChRM components not forced to the origin. All tick marks are 10^{-3} A/m. In (a), only component A is present, removed below 660°C. Specimens from component B (b) group generally unblock to the origin between 660 and 680°C with single-polarity directions, after removal of component A. Component C (c) unblocks to the origin between 660 and 680°C and has dual-polarity ChRM directions after removal of component A. (d) Specimens from the Lengjiaxi Group (below the conglomerate) contain component A, but not B or C.

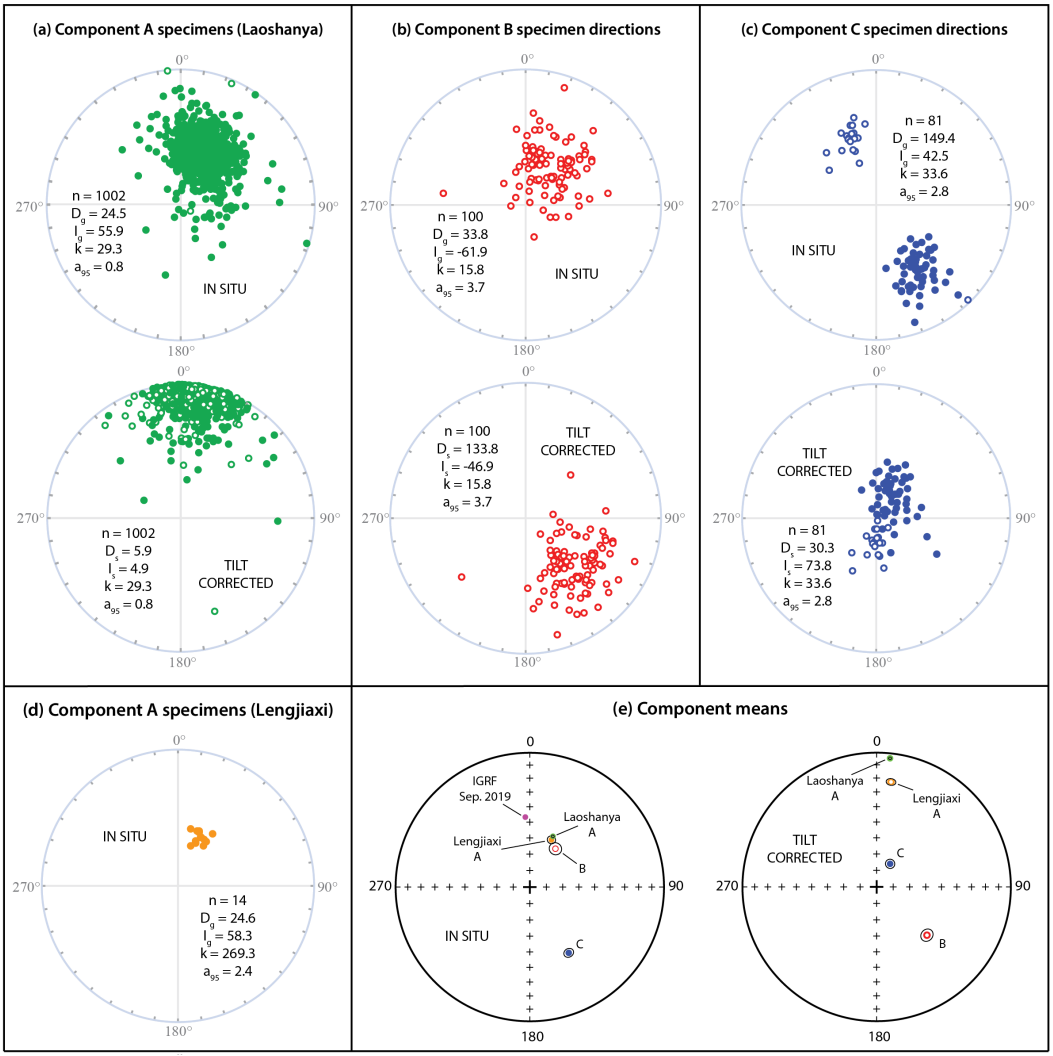

Figure 5. Stereonet plots of component A-C paleomagnetic directions in geographic (in situ) and stratigraphic (tilt-corrected) coordinates. Filled circles are lower hemisphere, open circles upper hemisphere. (a-c) Components A and B have a single-polarity while component C has dual-polarities. (d) Specimens from the Lengjiaxi Group only contain component A, indistinguishable to that from the Laoshanya Formation in geographic coordinates. (e) Component mean directions for components A, B and C are distinguishable from the expected IGRF direction (Alken et al., 2021). α_{95} ellipses are shown in black; α_{95} for Laoshanya A component is smaller than the point indicating the direction.

Component C (n = 81) comprises dual-polarity directions with steep inclinations in tilt corrected coordinates; 62 samples have positive inclinations and 19 negative (Fig. 5c). A reversal test (McFadden & McElhinny, 1990) is negative at the 95% confidence level. However, the reversal test is positive (B classification) if the specimens are filtered for the directions that decay linearly to the origin with maximum angular deviations (MAD) $\leq$ 10° (n = 44, Fig. S3). Large MAD values likely arise from unresolved overlapping components (B+C). Components B and C were only found in the Laoshanya Formation so no fold test could be performed at the local level. Below, we show the results of a regional fold test, which is negative for component B and positive for component C.

4.2.2 Sedimentology

Median bed thickness defines three distinct parts (Fig. 6a). In the lowermost 20 m, median bed thickness ranges from 0.10 to 0.25 m for sandstones and 0.05 to 0.10 m for siltstones. This part preserves abundant ripple marks, suggesting a shallow, tidal or near-shore environment. Between 20 and 54 m, the median thickness of the sandstone beds increases up to 0.35 m. This part contains graded bedding and some cross-bedding, indicating more energetic deposition. Median thickness increases towards the top of the section (54-85 m) for both siltstones (up to 0.35 m) and sandstones (up to 0.4 m) which could indicate a more stable, perhaps deeper, depositional environment; cross-bedding and ripple marks are absent. These three parts compare well with stratigraphic units 1-5 described by Yin et al. (2004).

We compared the paleomagnetic results against the stratigraphic log (Fig. 6a) to test the correlation between lithology and magnetization components. Specimens containing component B arise mainly in the siltstone and fine sandstone beds (59%), with 41% taken from coarse sandstone beds (Figs. 6b and c). 77% of the specimens having component C come from coarse sandstones, while 23% come from finer sediments. Component C appears more frequently in the middle part (20-54 m), while component B is more abundant in the bottom (0-20 m) and top (54-85 m) parts. The highest density of specimens containing component C occurs in the thick sandstone beds between 45 and 50 m. This is not an artefact of sampling density as the spacing between specimens was kept constant at 5-10 cm throughout the section.

4.2.3 Vector unmixing

To quantify component contributions to the NRM, we performed vector unmixing analyses (Tonti-Filippini & Gilder, 2023) on 1152 specimens from the Laoshanya Formation (Fig. 7). A goodness of fit (GOF) $\geq$ 70% was achieved for 640 specimens using the mean component directions from Table 1 and the median demagnetization curves derived by Tonti-Filippini and Gilder (2023), i.e., demagnetization data for more than half the specimens could be accurately modelled by superimposed contributions from components A, B and/or C. In the following sections, we grouped the specimens by their dominant component, i.e., the estimated component contribution must be at least $\sim$ 40 % of the total NRM to qualify for that component group. However, 98% of the specimens contain some combination of two or three of the components.

4.3 Rock magnetic results

Thermal remanence curves for group A samples gradually decay between 100 and 660°C (Figs. 4a and d), consistent with fine-grained or pigmentary hematite (Collinson, 1974). Those in groups B and C unblock in a narrow range between 660 and 680°C (Figs. 4b and c), consistent with crystalline hematite (Özdemir & Dunlop, 2002, 2005). To further characterize remanence carriers, we carried out rock magnetic experiments on fresh specimens from cores chosen to best represent component groups A, B, and C.

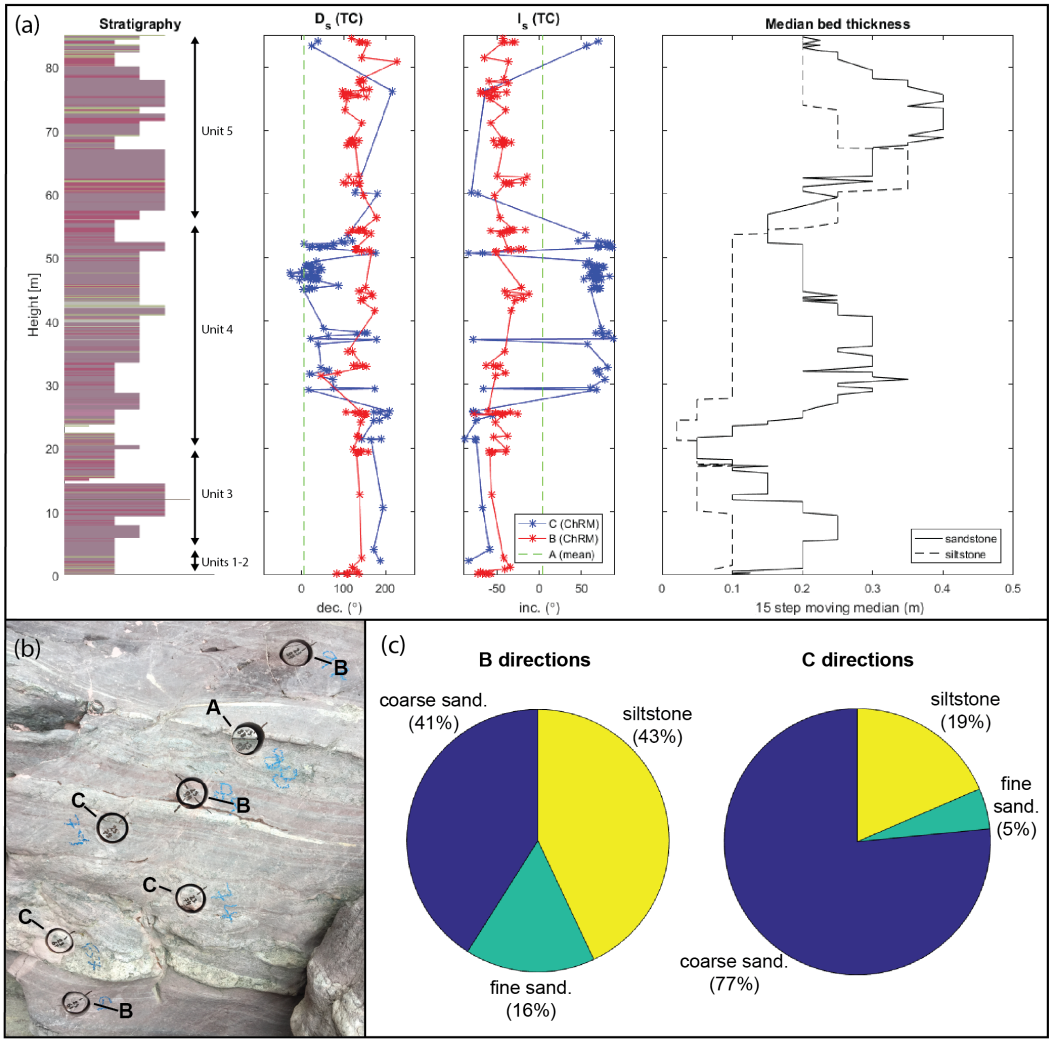

Figure 6. Lithological characteristics of paleomagnetic directions. (a) Graphical representation of the paleomagnetic section (Laoshanya Formation, Yangjiaping), with stratigraphic units identified by Yin et al. (2004). The section is shown alongside the paleomagnetic results (D_s and I_s = declination/inclination in stratigraphic [tilt corrected] coordinates) and median bed thickness by lithology. (b) Field photo of interbedded siltstone/sandstone that contain the components A-C as indicated. (c) Component C was more frequently identified in the coarse sandstone beds (nominal grain size > 250 µm), while component B was found more in the fine-grained sandstones (63 to 250 µm) and siltstones (< 63 µm).

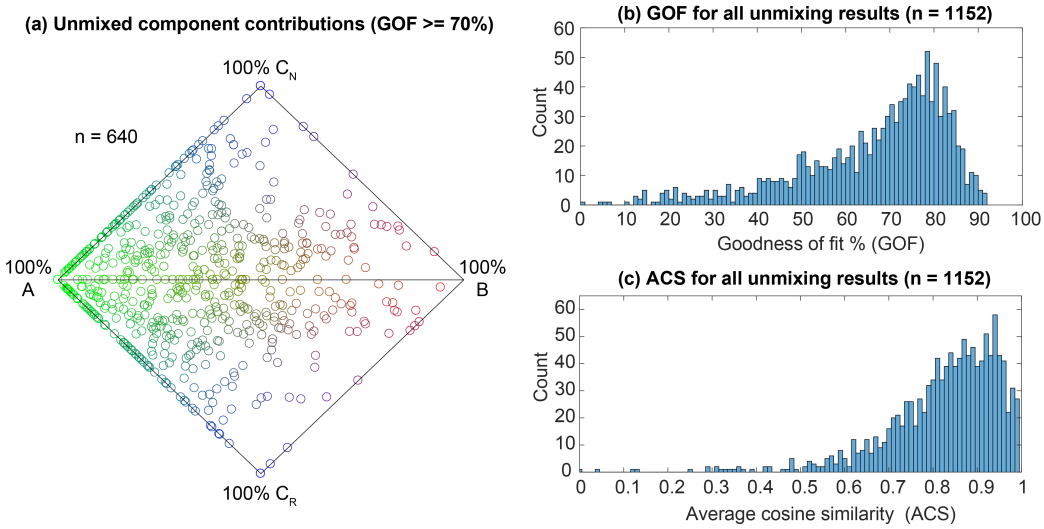

Figure 7. Results of vector unmixing analyses. (a) Specimen unmixing results with goodness of fit (GOF) $\geq$ 70 % (n = 640), shaded by component contribution where green = A, red = B and blue = C. Results are shown on a double ternary plot as a proportion of total NRM, unmixed using median component curves derived in Tonti-Filippini and Gilder (2023), representing estimated combinations of components A, B and C_N (positive inclinations) or C_R (negative inclinations). Distributions of (b) GOF and (c) average cosine similarity (ACS) for all Laoshanya unmixing results (n = 1152).

4.3.1 High temperature experiments

Fig. 8 shows representative magnetic susceptibility vs. temperature curves (9 out of 25 measured). All samples exhibit a rapid decline in susceptibility between 660 and 700°C, indicative of the Néel temperature in hematite. Another commonality, although variable in magnitude, is the existence of a phase with a Curie temperature around 100–200°C that is non-reversible upon cooling. This could be indicative of titanium-rich titanohematite, titanomagnetite or goethite.

The thermal susceptibility curves can be divided into three categories:

1. Samples in the first category (Figs. 8a-b, d-e and g) have reversible behavior with a Hopkinson peak around 660°C, characteristic of single-domain (SD) hematite grains (Dunlop, 1974).
2. Samples in the second category (Figs. 8c and h-i) have irreversible behavior upon cooling below 600°C, with a new or enhanced Hopkinson peak around 560°C, near the Curie temperature of magnetite. This is indicative of the creation of SD magnetite at high temperatures, which also explains the increase in bulk susceptibility above 600°C observed in the thermal demagnetization experiments; the susceptibility of magnetite is several orders of magnitude higher than hematite (O'Reilly, 1984).
3. The third category (Fig. 8f) has steep slopes in the cooling curves around 560-600°C, indicative of magnetite. However, the susceptibility of the cooling curves may be lower than the heating curves, suggesting some pre-existing magnetite was oxidized to hematite. At higher temperature, new magnetite was created, sometimes in lower concentration when the cooling curve is below the heating curve.

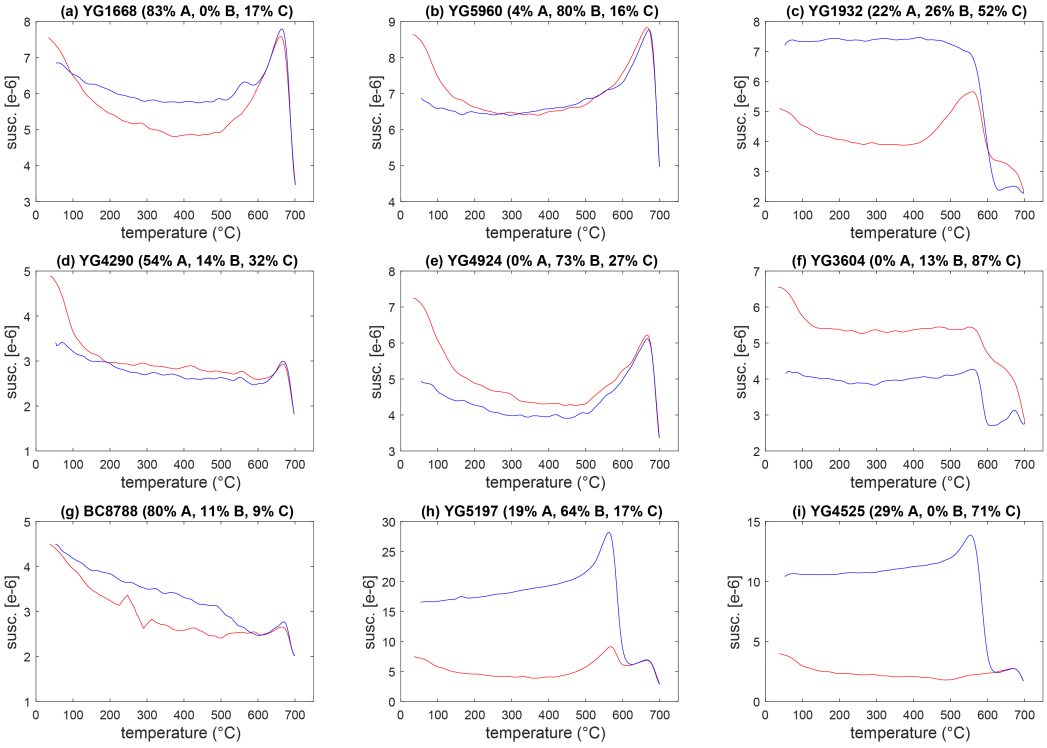

Figure 8. Susceptibility (not mass-normalized) vs. temperature curves for each component group between 20 and 700°C (in air) (red lines indicate heating, blue lines cooling). Component contributions estimated by vector unmixing analysis are shown in the subtitles. Most specimens show a Hopkinson peak around 660°C, with rapid decay up to 700°C, consistent with SD hematite. The Hopkinson peaks appear more pronounced in specimens with a dominant ($>$ 50%) component A (a, d, and g) or B (b, e, and h), compared to those with a dominant component C (c, f, and i). Some specimens, e.g., (c), (e) and (i), exhibit a Hopkinson peak upon cooling around 560°C, likely due to the creation of magnetite during heating. All samples have a phase with a Curie temperature below 150°C that is destroyed by heating, which may indicate the presence of high-Ti titanohematite, titanomagnetite or goethite.

4.3.2 Low temperature experiments

Low temperature experiments were performed on the VSM using a liquid nitrogen cryostat (Fig. S1). A magnetizing field of 1.8 T was applied at room temperature (293 K) then switched off. Magnetic remanence was then measured in a null field down to 100 K and then upon warming to room temperature at a rate of 0.25°/s. Pure hematite typically shows a drop in remanence through the Morin transition (Özdemir et al., 2008) around ∼250 K; however, none of the Yangjiaping samples displayed either a measurable Morin transition or a Verwey transition (characteristic of magnetite), at least until 100 K (note that temperature stability of the cryostat decreases approaching 100 K). Dekkers and Linssen (1989) observed similar low temperature behaviour in natural hematite and suggested that impurities (e.g., adsorbed silica) might suppress the Morin transition. Small amounts of Ti (e.g., 1 wt.%) can also suppress the Morin transition (Özdemir et al., 2008), so the absence of a measurable Morin transition is not uncommon. We found no evidence for a Verwey transition in the ca. 100-123 K range indicative of magnetite.

4.3.3 Hysteresis (VSM)

Hysteresis parameters were determined for 22 samples up to 1.5 T (Figs. 9a-b), although hematite can require >10 T to fully saturate (Rochette et al., 2005). Linear corrections (75-90% to 1.5 T) were subtracted to account for paramagnetic contributions. The corrected hysteresis loops for samples with dominant A or B components (Figs. 9c-d) are broad and do not saturate, consistent with single domain (SD) hematite (Özdemir & Dunlop, 2014). Samples in group C (Fig. 9e) show narrow wasp-waisted curves, indicating populations of grains with contrasting coercivity. These wasp-waisted loops are similar to multidomain (MD) hematite behaviour observed by Özdemir and Dunlop (2014). Compositional variations in titanohematite grains could also explain wasp-waisted hysteresis behaviour (A. P. Roberts et al., 1995), as can mixtures of magnetite and hematite.

Samples in group C have bulk coercivities (Hc) an order of magnitude lower and saturation magnetizations (Ms) $2-3$ times higher than those in groups A and B (Fig. 9f). Values of Hc between 10 and 100 mT in group C imply hematite grain sizes of 10-300 µm (Özdemir & Dunlop, 2014), while values between 300 and 600 mT (for groups A and B) imply smaller hematite grain sizes, on the order of d = 0.1-3.0 µm. However, we note that these numbers pertain to very crystalline hematite, and natural hematite can have a maximum in coercivity at a much smaller grain size. Kletetschka and Wasilewski (2002) estimated the SD to MD grain size transition at 100 µm for hematite, suggesting that the group C hematite is more MD rich than groups A and B. As would also be expected for MD hematite, most samples from group C have only minor or non-existent Hopkinson peaks (Fig. 8).

4.3.4 Anisotropy (AMS and AMR)

We measured the anisotropy of magnetic susceptibility (AMS) on 99 non-demagnetized core specimens (Figs. 10a-e and S2a-c). Anisotropy degrees (P) were <1.1, with maximum axes (K1) trending 235° on average in the horizontal plane (tilt-corrected coordinates). Intermediate (K2) and minimum (K3) axes spread over a NW-SE great circle, with some clustering in the vertical and horizontal planes. AMS directions are not markedly different among the three groups, although group C has a more pronounced tectonic fabric (Fig. 10c). The intermediate tectonic fabrics are typical of sedimentary rocks in thrust-and-fold belts (Saint-Bezar et al., 2002). However, the K2-K3 plane implies a 325° shortening direction (235°-trending fold axis), which differs from the measured strike of our section (255°) by 20° (Fig. 10e).

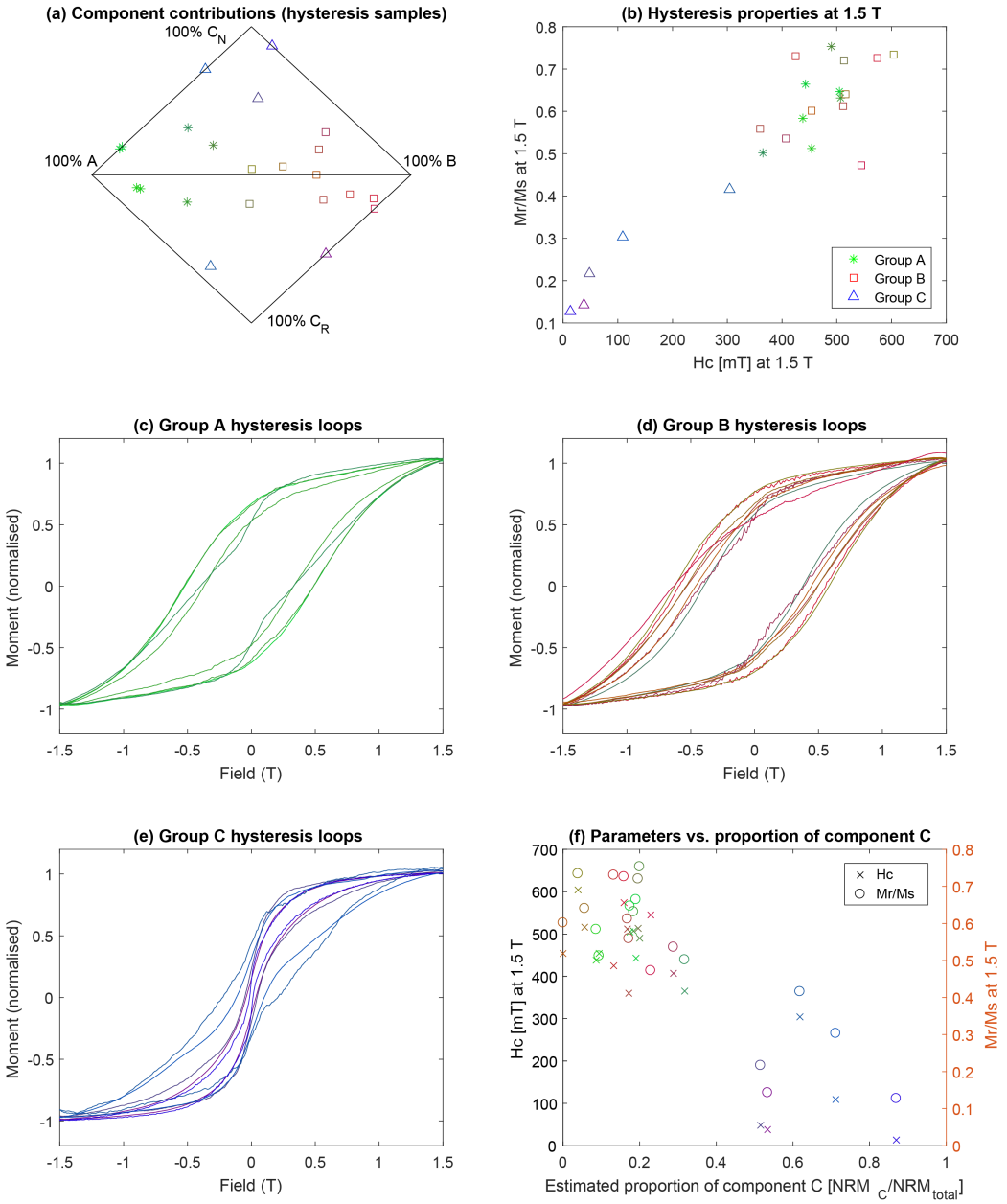

Figure 9. High field experiments. (a) Vector unmixing results for samples used in the hysteresis experiments, with dominant components indicated by blue triangles (C), red squares (B) and green stars (A). The same colour shading is preserved in b-f. (b) Samples with higher Mr/Ms ratios have higher coercive forces (Hc). Lower Hc values can indicate larger hematite grain sizes (Özdemir & Dunlop, 2014), and/or mixtures of magnetite with hematite. (c-e) Room temperature hysteresis curves for specimens from component groups A, B, and C. Groups A and B have wide curves consistent with single domain hematite. Group C has wasp-waisted loops, indicating populations of grains with distinctly different coercivity spectra. (f) Mr/Ms and Hc values (at 1.5 T) correlate negatively with the proportion of component C.

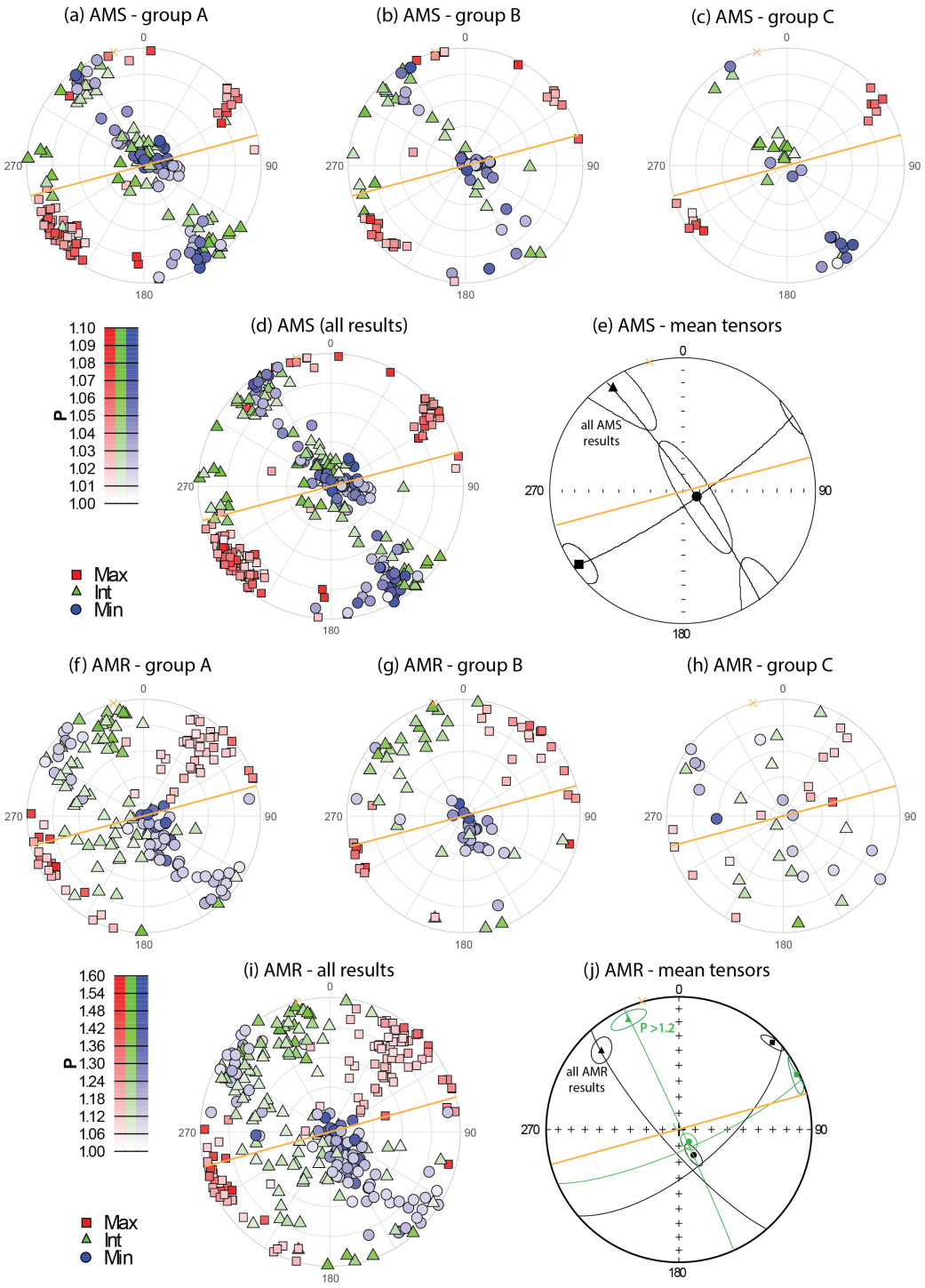

Figure 10. (Caption next page.)

Figure 10. (Previous page.) Stereonet plots of principal axes directions for anisotropy of magnetic susceptibility (AMS) and anisotropy of magnetic remanence (AMR) measured in Laoshanya samples. The strike in Yangjiaping is shown in orange. Symbols are shaded by anisotropy degree (P). Note the different scales between AMS and AMR. (a-c) AMS principal axes directions of the three component groups in tilt-corrected coordinates. Groups A and B have sedimentary fabrics (K3, the minor axis, lies perpendicular to the bedding plane) with varying degrees of a tectonic overprint. Maximum anisotropy axes (K1) lie approximately parallel to strike, while some K3 axes are rotated toward the horizontal along a great circle trending perpendicular to strike. Group C records a strong tectonic fabric, with horizontal K3 directions and K2 (intermediate axis) directions perpendicular to bedding. (d) AMS principal axes directions for all samples. (e) The mean K2-K3 plane defines a shortening direction oriented 325°. (f-h) AMR principal axes directions for groups A and B are generally compatible with those from AMS. Group C has mostly incoherent fabrics. (i) Taken together, the most anisotropic samples have AMR K1 directions that parallel more closely to the fold axis direction than AMS. (j) Mean AMR tensors divided by shape anisotropy. Samples with P >1.2 are more consistent with the regionally-defined compression axis (345°) – all results (black) = 316°, for P >1.2 (green) = 335°.

Anisotropy of magnetic remanence (AMR) was measured on the same 99 specimens (Figs. 10f-j and S2d-f) using the refinement method of Wack (2023). Groups A-C have similar fabrics as AMS, although more scattered (Figs. 10f-h). P values are generally <1.2 with mean principal axis directions are similar to those for AMS, with maximum axes (M1) declinations trending 227°, compared to 235° for AMS (K1). Considering all results together, 29 specimens have P >1.2 (mean P = 1.12 for n = 99). Mean M1 axes for those (P >1.2) specimens trend 245°, 20° clockwise relative to the total population (Figs. 10i-j). The more anisotropic specimens occur in groups A and B, suggesting they absorbed more of the tectonic stress that produced the deformation in Yangjiaping. This is not surprising since finer-grained sediments (Section 4.2.2) with higher clay contents typically absorb more tectonic strain (Kodama, 2012).

4.4 Mineralogy and microscopy

X-ray diffraction peaks are dominated by quartz (25-34 %), albite (12-20 %), muscovite (42-54 %) and chlorite (2-5 %) (e.g., Fig. S5). Hematite is the main iron-bearing mineral whose concentration varies from 2 to 6 wt.%. Chlorites also contain up to 4 % Fe (EDXS data). SEM observations and EDXS analyses accord well with the XRD data. SEM images show that fine-grained micas and silicates (chemically consistent with muscovite and chlorite) cluster around coarse grains of quartz and alkaline feldspar. Accessory minerals, such as vermiculite, calcite, apatite, zircon, monazite and rutile, were chemically characterized by EDXS.

SEM images (Fig. 11) show abundant hematite in all samples. Fine, needle-like hematite flakes, generally < 1 µm, are ubiquitous but more dominant in group A samples (Figs. 11a-f). Samples from groups B and C contain large (30–100 µm), Ti-rich hematite and martite (hematite pseudomorphic after magnetite) grains showing trellis textures of exsolution typical of Ti-magnetite and/or (hemo-)ilmenites (Figs. 11g-r). Samples from group B also show abundant 1–2 µm hematite platelets scattered throughout the matrix, or in dense clusters, which presumably replaced and/or oxidized Fe-rich grains (Figs. 11g-k). Larger grains in group B appear to be more leached, with empty Ti-rich (rutile) lattices left behind, surrounded by hematite platelets (Fig. 11l). Group C samples

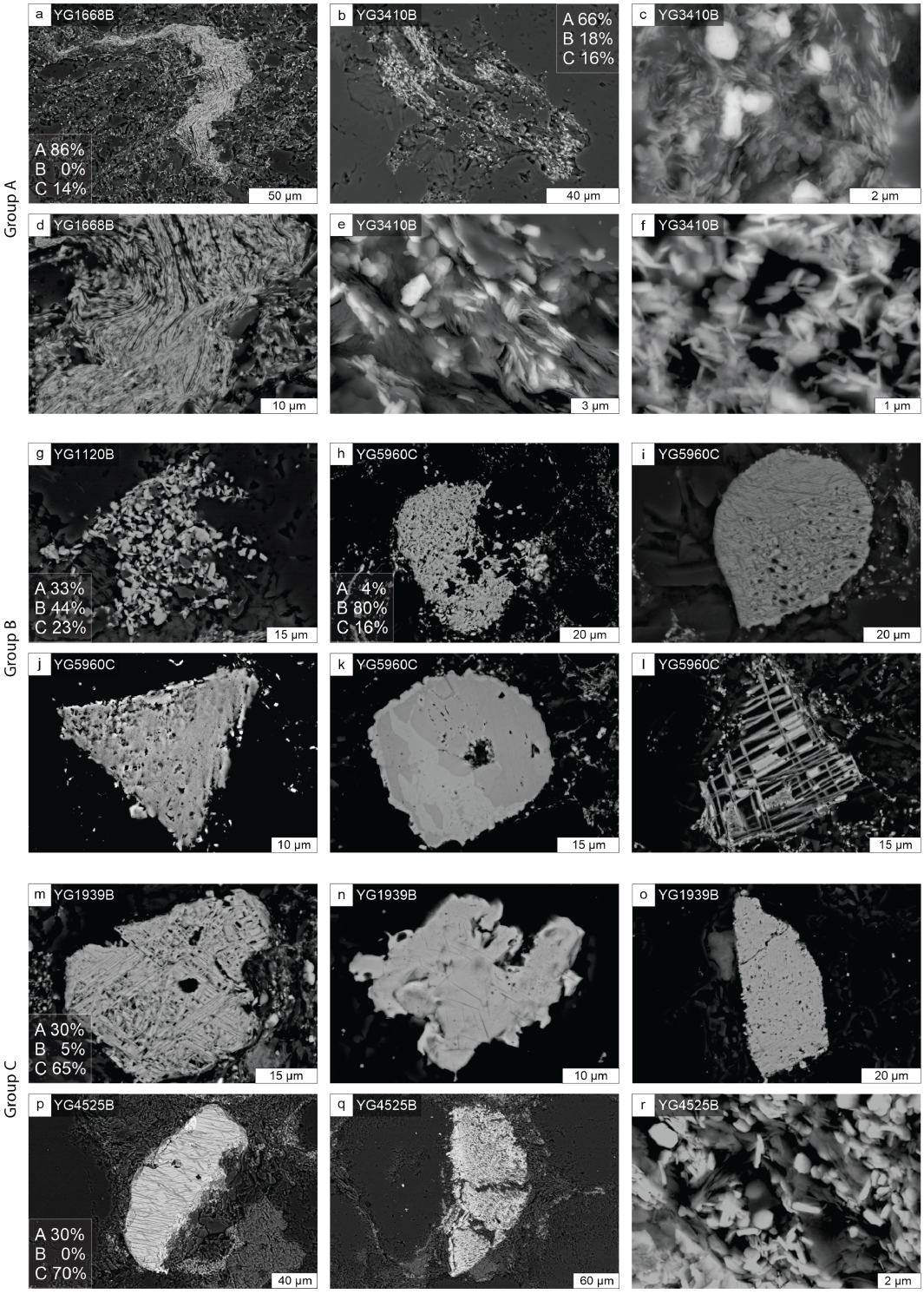

Figure 11. SEM images indicating component proportions estimated by vector unmixing analyses. (a-f) Specimens dominated by component A show pervasive Fe remobilization and fine, needle-like hematite flakes, generally <1 µm. (g-l) Component B-rich specimens contain dense clusters of hematite platelets ca. 1–2 µm which appear to have formed in situ, perhaps from the leaching of Ti-rich trellis structures. (m-r) Specimens with a high proportion of component C generally have fewer fine-grained hematite flakes and platelets, and are dominated by large (30-100 µm) Ti-rich hematite and martite grains with exsolution features typical of converted Ti-magnetite and/or (hemo-)ilmenite.

generally contain fewer hematite flakes in the matrix than the other sample groups (Figs. 11m-p), consistent with minimal Fe remobilization. Overall, these observations suggest there was greater Fe remobilization in groups A and B than in group C.

5 Interpretation and discussion

Our experimental results offer several insights into the nature of the remanent magnetizations in the Laoshanya Formation:

1. SEM analyses show that group C samples contain abundant detrital (ca. 30 – 100 µm) Ti-rich hematite grains indicative of MD grain sizes, consistent with an igneous or metamorphic source (Basu & Molinaroli, 1989), and therefore a primary/detrital remanence (DRM). These samples also contain a reduced presence of < 1-2 µm (SD-sized) hematite flakes relative to the samples from groups A and B. Hysteresis curves for group C samples appear wasp-waisted, indicating distinct magnetic populations or dominantly MD grains. Thermal-susceptibility curves for group C also showed minor to non-existent Hopkinson peaks, consistent with MD behaviour.
2. Hysteresis parameters suggest that samples from groups A and B are dominated by SD hematite. Thermal-susceptibility curves for groups A and B also show distinct Hopkinson peaks. The inference of SD hematite is further supported by SEM observations of abundant sub-micron hematite particles in these samples, consistent with Fe remobilization and secondary fluid circulation, potentially from the dissolution of Fe-rich minerals (Walker et al., 1981). The fact that the SEM images show the SD hematites to be secondary products supports a chemical formation, and hence, a CRM.
3. AMR fabrics indicate group A and B specimens may have absorbed more tectonic stress, with higher anisotropy and an inferred strain axis rotated 20° relative to the other component groups, consistent with higher clay content/more fine-grained material.

5.1 Components in the Laoshanya Formation

Of the three magnetization components isolated in this study, component A fails the fold test between the Laoshanya and Lengjiaxi formations. The corresponding direction at 0% unfolding is D = 24.5°, I = 55.9°, α_{95} = 0.8°, composed solely of normal polarity, similar to a widespread overprint component found throughout South China, originally described by Kent et al. (1987). The corresponding pole at lat = 68.6°N, lon = 176.7°E, dp/dm = 0.8°/1.1° is near-sided with respect to Cretaceous reference poles for South China. The unfolding path of component A intersects the Cretaceous poles of Huang et al. (2018) at 10-20% unfolding; however, the reference pole is based mostly on sedimentary rocks, which can be affected by inclination shallowing. Given that the overprint is a CRM and the reference poles are based mostly on continental sediments with DRM, one would expect a CRM to be immune from inclination shallowing, as found by Meng et al. (2022). Hence, we interpret component A to be a Cretaceous overprint acquired during the normal superchron [120-83 Ma (Ogg, 2012)].

The interpretation of components B and C is more complicated. Taken at face value, both components could be primary, as they display near-identical thermal remanence behaviour. Fig. 12 plots the corresponding poles in both geographic and stratigraphic coordinates, together with a 450 to 120 Ma APWP for South China (Huang et al., 2018). The component B pole in tilt-corrected (TC) coordinates [LS-B (TC)] lies in proximity to the 450 Ma segment of the reference APWP. Component B in geographic/in situ (IS) coordinates [LS-B (IS)] and the TC and IS poles for component C lie far from the reference curve.

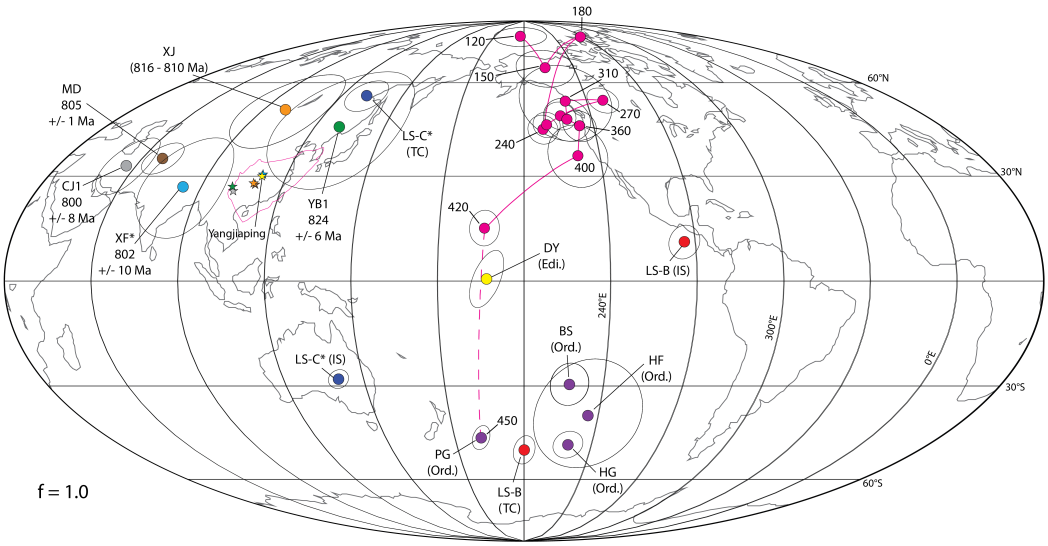

Figure 12. Laoshanya (LS) Formation poles from components B and C in in situ (IS) and tilt-corrected (TC) coordinates plotted with the APWP for South China from Huang et al. (2018) shown in pink. LS-C* and Tonian (820-800 Ma) poles are shown in normal (northern hemisphere) polarity for the sake of comparison, although an inverted (southern hemisphere) configuration is also possible (Jing et al., 2021). LS-B is shown in reversed (southern hemisphere) polarity as the LS-B (TC) pole lies close to the 450 Ma segment of the APWP (the line is dashed as there is only one study pole, PG, older than 420 Ma). LS-B (IS) and LS-C* (IS and TC) lie far from the reference path. Table S1 provides details of relevant Tonian poles (820-800 Ma). Ordovician (Ord.) poles are shown in purple (Table S2). The Ediacaran (Edi.) pole from the Doushantuo Formation in Yangjiaping (DY) is shown in yellow. Stars indicate site locations. No shallowing correction was applied for this initial comparison (f = 1.0).

Fig. 12 also plots our data alongside select Tonian to pre-Devonian poles from the SCB (Tables S1 and S2, assessed in Supporting Information [SI] Section B). LS-B (TC) lies among several Ordovician poles for the SCB. Together with the rock magnetic and microscopic observations (Section 4), we interpret component B to be an Ordovician-aged chemical remagnetization. This interpretation is consistent with a mineralogical study in Yangjiaping that indicates the Banxi Group may have experienced very low-grade metamorphism (ca. 260°C) in the mid-Paleozoic (H. Wang et al., 2014). Estimated temperatures increase to 360°C towards eastern Hunan and the Jiangnan belt, whose heat source was linked to the Wuyi-Yunkai (Caledonian) Orogeny (H. Wang et al., 2016). Moreover, Cawood et al. (2018) suggested that the Banxi Group and its equivalents in the Jiangnan belt were reworked between 460 – 420 Ma; this timing is supported by metamorphic and petrogenetic analyses together with $^{40}Ar/^{39}Ar$ and U-Pb dating across the Wuyi-Yunkai orogen (Z. X. Li et al., 2010).

The component C pole, LS-C* (TC), lies close to Tonian poles from the 824 ± 6 Ma Yanbian Dykes (Niu et al., 2016) and 816 – 810 Ma Xiajiang Group (Park et al., 2021). The similarity with other Tonian-aged poles, as well as its dual-polarity, lead us to interpret component C as primary. Reversal frequency in the Tonian (ca. 807.5 Ma) based on seven polarity intervals between 20 – 54 m (34 m), where the highest density of component C directions are found (Fig. 6a), yields 0.21 reversals per metre or 6.7 reversals/Myr (rev/Myr) given an accumulation rate of 32 m/Myr. This is a minimum value, as the true number could be higher if the signal was obscured by component A or B overprints. Our estimate for the Tonian is higher than the present rate of 4 – 5 rev/Myr for the past 5–10 Myr (Ogg, 2012), but is within estimated rates for the rest of the Phanerozoic, which often exceed 5 – 10 rev/Myr (Torsvik et al., 2021), and the Ediacaran at 6 – 24 rev/Myr (Meert et al., 2016; Hounslow et al., 2018). For comparison with other studies, we have grouped the component C directions into 'sites' of n=8–12 (Table S3), although we use the filtered specimen mean (n=44) to define our pole (LS-C*).

5.2 Paleomagnetic poles from South China

We assess relevant Tonian (820-800 Ma) poles in Section B (SI). We excluded poles CJ3 (Jing et al., 2020) and YB2 (Niu et al., 2016) because they lack reversals and fail the statistical requirements of Meert et al. (2020). Poles XJ, CJ1 and MD were derived from sedimentary rocks; Park et al. (2021) corrected these poles for inclination shallowing with a blanket flattening factor (f) of 0.6. However, none of these studies applied any E/I or anisotropy-based methods to justify this factor. We applied the E/I correction method (Tauxe & Kent, 2004) to Laoshanya component C directions (n = 81) but could not obtain a meaningful result (i.e. our data were labelled 'pathological'), which may be due to contamination by the component A and B overprints. Our E/I assessment of all 169 specimen data from Park et al. (2021) corrected the mean inclination from -72.5° to -75.7°, equivalent to f = 0.81, although we recognise that the E/I method may overestimate shallowing effects if applied to data spanning several sites (e.g., Meng et al., 2017). Therefore, we find it difficult to justify using f = 0.6. To estimate a flattening factor, we applied a range of f values on inclinations from sedimentary poles (CJ1, MD, XJ and LS-C*) from 1.0 to 0.6 and compared them to those from igneous poles (XF* and YB1), keeping the igneous inclinations fixed (Table S4). A value of f=0.8 produced the lowest standard deviation across all poles, so we used this value to correct the sedimentary poles. This assessment relies on an assumption that all the 820-800 Ma poles are coeval, which is discussed further below.

Fig. 12 shows that the Tonian poles appear to undergo high amplitude and rapid motion between 820 and 800 Ma, which some workers have previously interpreted as reflective of a rapid TPW oscillation (e.g., Z. X. Li et al., 2004; Niu et al., 2016; Jing et al., 2020). However, Park et al. (2021) showed that the arc distances between the ∼815 and ∼805 Ma (Xiajiang and Madiyi) poles are much smaller than what would be predicted by the

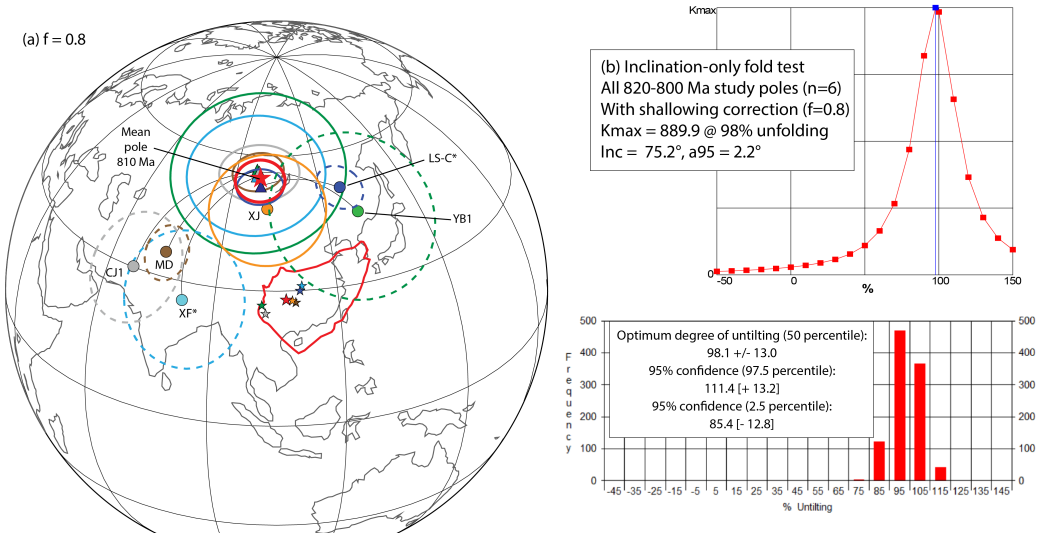

Figure 13. Scenario 1: Can vertical axis rotations explain discordant paleomagnetic data in the Tonian? (a) If allowed to rotate, all Tonian poles (820-800 Ma) collapse to define a group pole ca. 810 Ma. XJ was held fixed as its site location (and pole) lies between all the other sites (and poles). The outline of the SCB and the group mean pole are in red. Dashed circles indicate pole locations before vertical axis rotations. Poles are summarized in Table S1 and Section B (SI). (b) An inclination-only fold test with parametric sampling (Watson & Enkin, 1993; Enkin & Watson, 1996); k maximizes at $98 \pm 13\%$ unfolding.

Bitter Springs TPW hypothesis, although they considered that this could be explained by differential plate motion. Park et al. (2021) also described how the data could be interpreted to represent a stable high-latitude position for South China at ca. 825-805 Ma, inconsistent with rapid TPW, if the Svalbard data are removed as constraints. Our new data from Laoshanya supports this interpretation, as our ~808 Ma pole lies between the Xiajiang and Madiyi poles chronologically, but does not fall on the inferred TPW path. In fact, the pre-Bitter Springs Stage XJ pole and syn-Bitter Springs Stage LS-C* pole overlap within uncertainty after shallowing corrections are applied (Fig. 13). Furthermore, the Laoshanya (808 Ma) and Madiyi (805 Ma) formations are both precisely dated and very similar in age, but the poles are 50° apart, implying extremely rapid motion of ca. 17°/Myr, which is an order of magnitude greater than TPW rates estimated for the Phanerozoic (Torsvik et al., 2012). Therefore, in the following sections, we consider alternative hypotheses to explain the data.

5.2.1 Scenario 1: Vertical axis rotations dispel TPW

All the 820–800 Ma poles for South China show similarly steep inclinations, implying a high paleolatitude for the SCB (Fig. 12). We can be particularly confident in inclinations from sedimentary rocks, whose paleohorizontal can be robustly measured by the bedding attitudes. However, all paleomagnetic poles can be susceptible to uncertainty associated with vertical axis rotations, especially when going far back in time, like in the Precambrian. Vertical axis rotations can lead to poles distributed along small circles centered on the sampling sites, as shown in Fig. 13(a). Therefore, the large changes in declination can be explained without the need for IITPW, if rotations are permitted. Although the interior of South China experienced only minor rotations (<20°) since the Cretaceous (Meng et al., 2022), Permo-Triassic rocks exhibit a large variability in

declination that matches the rotational amplitude of the Tonian data (Tan et al., 2007; Gilder et al., 2008). We therefore entertain the possibility in Scenario 1 that the SCB experienced internal vertical axis block rotations that streaked the Tonian poles out about a small circle centered on the sampling sites.

Under this scenario, all poles are considered to be based on primary, approximately coeval magnetizations, obtained at similar paleolatitudes. We arbitrarily kept XJ fixed as it passed a regional fold test and its site and pole lie in the middle of the other sites and poles. After allowing the other 820-800 Ma poles to freely rotate about their respective sampling sites, the poles come into close coincidence (Fig. 13a). If the data were primary, a regional fold test on the directions would be meaningless given the dispersion in declination, yet an inclination-only fold test would be independent of the differential rotations. An inclination-only fold test (Enkin & Watson, 1996) yielded a maximum precision parameter κ_{max} at $98 \pm 13\%$ unfolding with an inclination of 75.2° (Fig. 13b). Therefore, by accounting for vertical axis rotations, the 820-800 Ma South China poles can be explained without the need to invoke rapid TPW, extreme plate motion or anomalous field behaviour. Assuming that Xiajiang is representative of the overall continent (without vertical axis rotation), we thus calculate a mean pole of $P_{lat} = 54.1°$, $P_{lon} = 99.0°$ ($A_{95} = 5.0°$, N = 6 studies) which we consider representative of the Tonian for the SCB at ca. 810 Ma.

The rotations required by Scenario 1 are quite large (over 90° between CJ1 and LS-C/YB1), so it is worth considering whether these are realistic with respect to the tectonics of South China. The structural framework of the Yangtze craton is dominated by a large curved orocline, readily observed in regional maps and satellite imagery. Tan et al. (2007) and Gilder et al. (2008) showed that this trend is reflected in paleomagnetic directions from late Permian to Middle Triassic rocks in South China. Differences in rotations can exceed 180° among sites when integrating over the past ca. 300 Myr. Rotation magnitudes could be even more dispersed when integrated over an additional 500 Myr.

5.2.2 Scenario 2: Pervasive Ordovician remagnetization

In Scenario 2, we consider the possibility that remagnetization is pervasive in the SCB. We fit a small circle running through three, presumably primary Ordovician poles (HF, HG and BS), centered on their mean site location (Fig. 14a). When plotted in the southern hemisphere, the 'Tonian' CJ1, MD and XF* poles lie near the small circle swath, suggesting that Ordovician remagnetization may be a common feature that better explains the origin of their remanences. Indeed, the Madiyi (MD) pole was derived from silty mudstones, like component B in the Laoshanya Formation. This is curious, as silty mudstones can carry primary detrital remanences, as revealed through intraclast conglomerate tests (Tauxe et al., 1980; Opdyke & DiVenere, 2004; Swanson-Hysell et al., 2019). The Chengjiang (CJ1) study also reports a mid-inclination secondary component (CJ3) which is offset from the primary component (à la Laoshanya components B and C). Therefore, an Ordovician remagnetization advocated in Scenario 2 provides an alternative explanation for the differences in pole positions ca. 805 Ma, whereby some of the magnetization components are wholly or partially overprinted. Instead of large amplitude and rapid TPW, there could be mixing of components acquired at distinctly different times.

Remagnetization could have occurred during a mid-Paleozoic deformation event (i.e. the Wuyi-Yunkai Orogeny). Consistent with this idea, Chang et al. (2022) mapped the Banxi Group as unconformably overlain by Devonian strata, thereby supporting an Ordovician-Silurian deformation event. 90 km to the south-east of Yangjiaping, an angular unconformity occurs at the top of the Middle Ordovician Guniutan Formation (Schmitz et al., 2010), however, near Yangjiaping, the formations above and below the

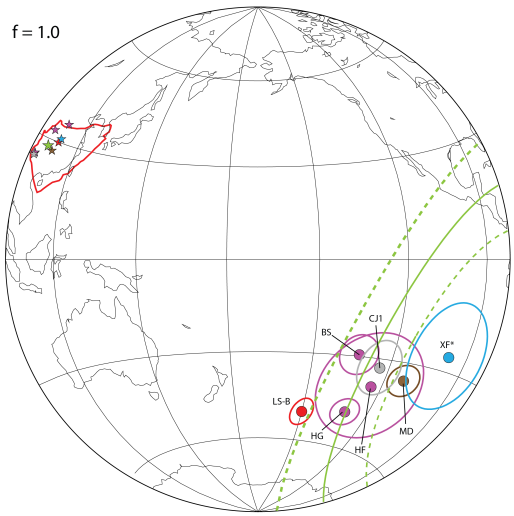

Figure 14. Scenario 2: Can an Ordovician remagnetization account for the discordant directions in South China? When plotted in the southern hemisphere, the CJ1, MD and XF* poles (Table S1) overlap with several Ordovician poles (purple, see Table S2), suggesting they may be affected by Ordovician remagnetization. No corrections for inclination shallowing were applied in this comparison (f=1.0). A small circle (green) is plotted through HF, HG and BS poles, centered on the mean site location (PG was excluded from the small circle calculation as it has a significantly different inclination). Dashed lines show 95% confidence limits.

Guniutan Formation have similar bedding orientations. Chen et al. (2014) described a significant hiatus between the Ordovician Wufeng and Silurian Longmaxi (Lungmachi) formations in Zhangjiajie, 100 km south of Yangajiaping. Zheng et al. (2020) dated the onset of this hiatus to 447 ± 1.4 Ma using rhyolitic tuffs in the top of the Wufeng Formation, 30 km to the north of Yangajiaping, and linked the hiatus to deformation/uplift caused by the Wuyi-Yunkai Orogeny. An Ordovician age for the deformation and remagnetization is consistent with the apparent age of component B in the Laoshanya Formation, as its pole overlaps several Ordovician poles.

5.3 Summary of discussion

We show that rapid pole variations postulated for ca. 820-800 Ma can be explained by vertical axis rotations and/or regional remagnetization in South China, without invoking extreme plate motion, rapid TPW or abnormal field geometry. South China's poles for this time are distributed along a small circle centered on the mean site location and can be brought into close alignment if vertical axis rotations are permitted. Furthermore, some poles derived from Tonian-aged rocks lie within a swath of Ordovician poles (when plotted in the same hemisphere), leading us to conclude that paleomagnetic data from other Madiyi-equivalent formations may reflect a regional overprint, not primary remanences. A complicated mixture of primary and secondary magnetizations may have led some studies to support a rapid TPW (or IITPW) event. Similarity between South China's Tonian and Ordovician paleolatitudes could be contributing to the confusion, if an Ordovician remagnetization is widespread.

Our results call for careful consideration of paleomagnetic signals in sedimentary sequences containing diverse lithologies, particularly those with hematite-bearing (red) mudstones and sandstones. Further work is needed to unravel the response of the Yangtze

craton to the Wuyi-Yunkai Orogeny and understand mechanisms for (re)magnetization of pre-Silurian strata. If the discordant poles are indeed artefacts of a tectono-thermal event in the Ordovician, then any proposed remagnetization mechanism must be capable of resetting or overprinting paleomagnetic signals across a range of lithologies and magnetic mineralogies, as is also true for the Cretaceous overprint component.

6 Conclusions

The Laoshanya Formation in Yangjiaping contains a complicated paleomagnetic record which offers a unique opportunity to investigate remanence acquisition processes in hematite-bearing sedimentary rocks. Remarkably, the red beds seem to have preserved a primary (depositional) Tonian signal (component C), as well as secondary magnetizations residing in hematite created in the Ordovician (B) and/or Cretaceous (A). From our study we conclude the following:

1. Stepwise thermal demagnetization of 1152 samples isolated three end-member magnetization components (A-C) that combine in a complex and out-of-sequence manner throughout the 85 m of sampled section. Vector unmixing identifies the proportions of the three components, which are distinguished by their rock magnetic characteristics and microscopy, and may respectively represent the most common hematite phases found in red beds: pigmentary coatings, intergranular authigenic grains, and detrital specularite grains.
2. Component A is an overprint acquired during the Cretaceous normal superchron, a common direction found throughout South China. Thermal remanence curves for this component are consistent with fine-grained or pigmentary hematite, assumed to have formed by the oxidation of Fe-rich minerals. This interpretation is consistent with rock magnetic experiments and microscopic observations of abundant (< 1 µm) hematite flakes and needles in all specimens.
3. Component B is found mostly in fine-grained beds and likely formed authigenically at temperatures up to 260°C in Yangjiaping, and up to 360°C in Tonian-aged red beds farther south. In the Laoshanya Formation, the component resides in fine idiomorphic hematite crystals (1–2 µm) and/or in dense clusters/pseudomorphs of microplaty hematite. The corresponding pole lies near several Ordovician poles from the SCB, suggesting that the age of magnetic acquisition is Ordovician. We link component B to a regional low-grade tectono-thermal (< 260°C) event in the late Ordovician, which may have partially or fully remagnetized pre-Silurian formations on the Yangtze craton.
4. Component C is carried mostly by coarse-grained hematite and is interpreted to be a primary remanence based on a positive reversal test. High-precision U-Pb dating of zircons extracted from two tuff horizons in the section yielded dates of 807.52 ± 0.18/0.27/0.91 Ma and 804.50 ± 0.22/0.30/0.91 Ma, which constrain the depositional age of the section between 809 and 804 Ma (using linear extrapolation). The primary nature of Component C is further supported by its agreement with some coeval poles from South China. Our new pole supports a stable, high-latitude position for the SCB between 809 and 804 Ma, and therefore a peripheral location with respect to the Rodinia supercontinent.
5. A stable position for the SCB likely extends further back and forth in time, as differences in paleomagnetic poles between 820 and 800 Ma can be explained by vertical axis rotations and/or regional remagnetization. This inferred stability is therefore inconsistent with the hypothesized Bitter Springs TPW event.

Acknowledgments

This work was supported by the German Research Foundation (DFG grant GI712/18-1), the LMU-China Academic Network (LMU-ChAN), the National Natural Science Foundation of China (no. 41874076 and no. 41888101), and a Swiss Government Excellence Scholarship. We thank Yuyang Hu, Zhaoyang Zhou and Junjie Xu for their assistance in the field. We thank Leon Kaub, Petter Silkoset, Claudia Trepmann, Uwe Kirscher, Erwin Appel, Maria Ovtcharova, Aurélia Crinière, Sophie Nowak and Imène Esteve for assistance in their respective laboratories. We thank Ann Hirt for useful discussions and Yuchen Chi for assistance with translations and geological maps. SG expresses deep gratitude to Qirui Zhang for introducing him to the Yangjiaping Section in 1990 and to Qirui's family for moral sustenance. We thank the reviewers, Joseph Meert and Nicholas Swanson-Hysell, and the editors, Mark Dekkers and Daniel Pastor-Galán, for their constructive suggestions which improved our work.

Author contributions

BR and SG jointly conceived of the idea for this project and wrote the funding proposal together. JT, BR, EM, MW, SG and XZ carried out initial fieldwork in 2019. JM carried out supplementary sampling in 2021. JT was responsible for paleomagnetic and rock magnetic measurements with significant input from SG. EM, FD and JT were jointly responsible for the microscopic observations and mineralogical analyses. JT and AP carried out sample preparation and U-Pb geochronology with supervision by US. JT wrote the manuscript with significant input from BR and SG, and in consultation with the other authors. All authors have read and approved the final manuscript.

Open Research

Paleomagnetic data (Tonti-Filippini et al., 2024) are available in the MagIC database: `https://earthref.org/MagIC/19728`. DOI: 10.7288/V4/MAGIC/19728.

References

Alken, P., Thébault, E., Beggan, C. D., Amit, H., Aubert, J., Baerenzung, J., ... Zhou, B. (2021). International Geomagnetic Reference Field: the thirteenth generation. *Earth, Planets and Space*, *73*(1). doi: 10.1186/s40623-020-01288-x

Basu, A., & Molinaroli, E. (1989). Provenance characteristics of detrital opaque Fe-Ti oxide minerals. *Journal of Sedimentary Petrology*, *59*(6), 922–934. doi: 10.1306/212F90B6-2B24-11D7-8648000102C1865D

Blaauw, M., & Christeny, J. A. (2011). Flexible paleoclimate age-depth models using an autoregressive gamma process. *Bayesian Analysis*, *6*(3), 457–474. doi: 10.1214/11-BA618

Butler, R. F. (1992). *Paleomagnetism: Magnetic domains to geologic terranes*. Boston: Blackwell.

Cawood, P. A., Wang, W., Zhao, T., Xu, Y., Mulder, J. A., Pisarevsky, S. A., ... Zi, J. W. (2020). Deconstructing South China and consequences for reconstructing Nuna and Rodinia. *Earth-Science Reviews*, *204*, 103169. doi: 10.1016/j.earscirev.2020.103169

Cawood, P. A., Wang, Y., Xu, Y., & Zhao, G. (2013). Locating South China in Rodinia and Gondwana: A fragment of greater India lithosphere? *Geology*, *41*(8), 903–906. doi: 10.1130/G34395.1

Cawood, P. A., Zhao, G., Yao, J., Wang, W., Xu, Y., & Wang, Y. (2018). Reconstructing South China in Phanerozoic and Precambrian supercontinents. *Earth-Science Reviews*, *186*, 173–194. doi: 10.1016/j.earscirev.2017.06.001

Chang, L., Zhang, S., Li, H., Xian, H., Wu, H., & Yang, T. (2022). New paleomagnetic insights into the Neoproterozoic connection between South China and India and their position in Rodinia. *Geophysical Research Letters*, *49*(10). doi: 10.1029/2022GL098348

Charvet, J. (2013). The Neoproterozoic-Early Paleozoic tectonic evolution of the South China Block: An overview. *Journal of Asian Earth Sciences*, *74*, 198–209. doi: 10.1016/j.jseaes.2013.02.015

Chen, X., Fan, J. X., Chen, Q., Tang, L., & Hou, X. D. (2014). Toward a stepwise Kwangsian Orogeny. *Science China Earth Sciences*, *57*(3), 379–387. doi: 10.1007/s11430-013-4815-y

Cohen, K., Finney, S., Gibbard, P., & Fan, J.-X. (2013). The ICS International Chronostratigraphic Chart. *Episodes*, *36*(3), 199–204. doi: 10.18814/epiiugs/2013/v36i3/002

Collinson, D. W. (1974). The role of pigment and specularite in the remanent magnetism of red sandstones. *Geophysical Journal of the Royal Astronomical Society*, *38*(2), 253–264. doi: 10.1111/j.1365-246X.1974.tb04119.x

Condon, D. J., Schoene, B., McLean, N. M., Bowring, S. A., & Parrish, R. R. (2015). Metrology and traceability of U-Pb isotope dilution geochronology (EARTHTIME Tracer Calibration Part I). *Geochimica et Cosmochimica Acta*, *164*, 464–480. doi: 10.1016/j.gca.2015.05.026

Dekkers, M. J., & Linssen, J. H. (1989). Rockmagnetic properties of fine-grained natural low-temperature haematite with reference to remanence acquisition mechanisms in red beds. *Geophysical Journal International*, *99*(1), 1–18. doi: 10.1111/j.1365-246X.1989.tb02012.x

Driscoll, P. E. (2016). Simulating 2 Ga of geodynamo history. *Geophysical Research Letters*, *43*(11), 5680–5687. doi: 10.1002/2016GL068858

Dunlop, D. J. (1974). Thermal enhancement of magnetic susceptibility. *Journal of Geophysics*, *40*(1), 439–451.

Edward, O., Paul, A. N., Bucher, H., Vérard, C., Adatte, T., Sonke, J. E., ... Vennemann, T. (2023). Timing and Provenance of Volcanic Fluxes Around the Permian-Triassic Boundary Mass Extinction in South China: U-Pb Zircon Geochronology, Volcanic Ash Geochemistry and Mercury Isotopes. *Geochemistry, Geophysics, Geosystems*, *24*(6). doi: 10.1029/2023GC010912

Enkin, R. J., & Watson, G. S. (1996). Statistical analysis of palaeomagnetic inclination data. *Geophysical Journal International*, *126*(2), 495–504. doi: 10.1111/j.1365-246X.1996.tb05305.x

Evans, D. A. (2003). True polar wander and supercontinents. *Tectonophysics*, *362*(1-4), 303–320. doi: 10.1016/S0040-1951(02)00642-X

Evans, D. A. (2021). Meso-Neoproterozoic Rodinia supercycle. *Ancient Supercontinents and the Paleogeography of Earth*, 549–576. doi: 10.1016/b978-0-12-818533-9.00006-0

Evans, D. A., Li, Z. X., & Murphy, J. B. (2016). Four-dimensional context of Earth's supercontinents. In Z. X. Li, D. A. D. Evans, & J. B. Murphy (Eds.), *Supercontinent cycles through earth history* (Vol. 424, pp. 1–14). The Geological Society of London. doi: 10.1144/SP424.12

Eyster, A., Weiss, B. P., Karlstrom, K., & Macdonald, F. A. (2020). Paleomagnetism of the Chuar Group and evaluation of the late Tonian Laurentian apparent polar wander path with implications for the makeup and breakup of Rodinia. *Bulletin of the Geological Society of America*, *132*(3-4), 710–738. doi: 10.1130/B32012.1

Fisher, R. (1953). Dispersion on a sphere. *Proceedings of the Royal Society*, *217*, 295–305. doi: 10.1098/rspa.1953.0064

Gerstenberger, H., & Haase, G. (1997). A highly effective emitter substance for mass spectrometric Pb isotope ratio determinations. *Chemical Geology*, *136*(3-4), 309–312. doi: 10.1016/S0009-2541(96)00033-2

Gilder, S. A., & Courtillot, V. (1997). Timing of the North-South China collision from

new middle to late Mesozoic paleomagnetic data from the North China Block. *Journal of Geophysical Research: Solid Earth*, *102*(B8), 17713–17727. doi: 10.1029/97jb01201

Gilder, S. A., Leloup, P. H., Courtillot, V., Chen, Y., Coe, R. S., Zhao, X., ... Zhu, R. (1999). Tectonic evolution of the Tancheng-Lujiang (Tan-Lu) fault via Middle Triassic to Early Cenozoic paleomagnetic data. *Journal of Geophysical Research: Solid Earth*, *104*(B7), 15365–15390. doi: 10.1029/1999JB900123

Gilder, S. A., Tan, X., Bucher, H., Kuang, G., & Yin, J. (2008). Optimization of apparent polar wander paths: An example from the South China plate. *Physics of the Earth and Planetary Interiors*, *169*(1-4), 166–177. doi: 10.1016/j.pepi.2008.07.016

Halverson, G. P., Shen, C., Davies, J. H., & Wu, L. (2022). A Bayesian approach to inferring depositional ages applied to a late Tonian reference section in Svalbard. *Frontiers in Earth Science*, *10*. doi: 10.3389/feart.2022.798739

Hoffman, P. F., Kaufman, A. J., Halverson, G. P., & Schrag, D. P. (1998). A Neoproterozoic Snowball Earth. *Science*, *281*(5381), 1342–1346. doi: 10.1126/science.281.5381.1342

Hounslow, M. W., Domeier, M., & Biggin, A. J. (2018). Subduction flux modulates the geomagnetic polarity reversal rate. *Tectonophysics*, *742-743*, 34–49. doi: 10.1016/j.tecto.2018.05.018

Huang, B., Yan, Y., Piper, J. D., Zhang, D., Yi, Z., Yu, S., & Zhou, T. (2018). Paleomagnetic constraints on the paleogeography of the East Asian blocks during Late Paleozoic and Early Mesozoic times. *Earth-Science Reviews*, *186*(5), 8–36. doi: 10.1016/j.earscirev.2018.02.004

Jing, X., Evans, D. A., Yang, Z., Tong, Y., Xu, Y., & Wang, H. (2021). Inverted South China: A novel configuration for Rodinia and its breakup. *Geology*, *49*(4), 463–467. doi: 10.1130/G47807.1

Jing, X., Yang, Z., Evans, D. A., Tong, Y., Xu, Y., & Wang, H. (2020). A pan-latitudinal Rodinia in the Tonian true polar wander frame. *Earth and Planetary Science Letters*, *530*, 115880. doi: 10.1016/j.epsl.2019.115880

Kent, D. V., Zeng, X., Zhang, W. Y., & Opdyke, N. D. (1987). Widespread late Mesozoic to recent remagnetization of Paleozoic and lower Triassic sedimentary rocks from South China. *Tectonophysics*, *139*(1-2), 133–143. doi: 10.1016/0040-1951(87)90202-2

Kirschvink, J. L. (1980). The least-squares line and plane and the analysis of palaeomagnetic data. *Geophysical Journal of the Royal Astronomical Society*, *62*(3), 699–718. doi: 10.1111/j.1365-246X.1980.tb02601.x

Kirschvink, J. L., Ripperdan, R. L., & Evans, D. A. (1997). Evidence for a large-scale reorganization of Early Cambrian continental masses by inertial interchange true polar wander. *Science*, *277*(5325), 541–545. doi: 10.1126/science.277.5325.541

Kletetschka, G., & Wasilewski, P. J. (2002). Grain size limit for SD hematite. *Physics of the Earth and Planetary Interiors*, *129*(1-2), 173–179. doi: 10.1016/S0031-9201(01)00271-0

Kodama, K. P. (2012). *Paleomagnetism of Sedimentary Rocks: Process and Interpretation*. John Wiley and Sons. doi: 10.1002/9781118384138

Kodama, K. P. (2013). Grand challenges in geomagnetism and paleomagnetism. *Frontiers in Earth Science*, *1*, 1–3. doi: 10.3389/feart.2013.00003

Lan, Z., Li, X. H., Zhu, M., Zhang, Q., & Li, Q. L. (2015). Revisiting the Liantuo Formation in Yangtze Block, South China: SIMS U-Pb zircon age constraints and regional and global significance. *Precambrian Research*, *263*, 123–141. doi: 10.1016/j.precamres.2015.03.012

Li, C., Wang, X., He, C., Wu, X., Kong, Z., & Li, X. (2017). China National Digital Geological Map (Public Version at 1:200000 Scale) Spatial Database. *Geology in China*, *46*, 1–14. doi: 10.23650/data.A.2019.NGA120157.K1.1.1.V1

Li, D., Yang, Z., Liu, Y., Yang, K., Wu, D., & Cai, P. (2022). Timing and provenance transition of the Neoproterozoic Wuling Unconformity and Xihuangshan

Unconformity of the Yangtze Block: Responses to peripheral orogenic Events. *Minerals*, *12*(5), 1–27. doi: 10.3390/min12050596

Li, S., Cao, J., Feng, Z., Liu, X., Qin, Y., Hu, R., & Wang, C. (2022). Neoproterozoic to Palaeozoic tectonic deformation history of the western Jiangnan Orogen, South China: Insights from new structural and geochronological data from northern Guangxi. *Geological Journal*, *57*(1), 292–316. doi: 10.1002/gj.4298

Li, Z. X., Bogdanova, S. V., Collins, A. S., Davidson, A., De Waele, B., Ernst, R. E., ... Vernikovsky, V. (2008). Assembly, configuration, and break-up history of Rodinia: A synthesis. *Precambrian Research*, *160*(1-2), 179–210. doi: 10.1016/j.precamres.2007.04.021

Li, Z. X., Evans, D. A., & Halverson, G. P. (2013). Neoproterozoic glaciations in a revised global palaeogeography from the breakup of Rodinia to the assembly of Gondwanaland. *Sedimentary Geology*, *294*, 219–232. doi: 10.1016/j.sedgeo.2013.05.016

Li, Z. X., Evans, D. A., & Zhang, S. (2004). A 90° spin on Rodinia: Possible causal links between the Neoproterozoic supercontinent, superplume, true polar wander and low-latitude glaciation. *Earth and Planetary Science Letters*, *220*(3-4), 409–421. doi: 10.1016/S0012-821X(04)00064-0

Li, Z. X., Li, X. H., Wartho, J. A., Clark, C., Li, W. X., Zhang, C. L., & Bao, C. (2010). Magmatic and metamorphic events during the early Paleozoic Wuyi-Yunkai orogeny, southeastern South China: New age constraints and pressure-temperature conditions. *Bulletin of the Geological Society of America*, *122*(5-6), 772–793. doi: 10.1130/B30021.1

Macouin, M., Ader, M., Moreau, M. G., Poitou, C., Yang, Z., & Sun, Z. (2012). Deciphering the impact of diagenesis overprint on negative δ 13 C excursions using rock magnetism: Case study of Ediacaran carbonates, Yangjiaping section, South China. *Earth and Planetary Science Letters*, *351-352*, 281–294. doi: 10.1016/j.epsl.2012.06.057

Macouin, M., Besse, J., Ader, M., Gilder, S. A., Yang, Z., Sun, Z., & Agrinier, P. (2004). Combined paleomagnetic and isotopic data from the Doushantuo carbonates, South China: Implications for the "snowball Earth" hypothesis. *Earth and Planetary Science Letters*, *224*(3-4), 387–398. doi: 10.1016/j.epsl.2004.05.015

Maloof, A. C., Halverson, G. P., Kirschvink, J. L., Schrag, D. P., Weiss, B. P., & Hoffman, P. F. (2006). Combined paleomagnetic, isotopic, and stratigraphic evidence for true polar wander from the Neoproterozoic Akademikerbreen Group, Svalbard, Norway. *Bulletin of the Geological Society of America*, *118*(9-10), 1099–1124. doi: 10.1130/B25892.1

McElhinny, M. W. (1964). Statistical significance of the fold test in paleomagnetism. *Geophysical Journal of the Royal Astronomical Society*, *8*, 338–340. doi: 10.1111/j.1365-246X.1964.tb06300.x

McFadden, P. L., & McElhinny, M. W. (1990). Classification of the reversal test in palaeomagnetism. *Geophysical Journal International*, *103*(3), 725–729. doi: 10.1111/j.1365-246X.1990.tb05683.x

McLean, N. M., Condon, D. J., Schoene, B., & Bowring, S. A. (2015). Evaluating uncertainties in the calibration of isotopic reference materials and multi-element isotopic tracers (EARTHTIME Tracer Calibration Part II). *Geochimica et Cosmochimica Acta*, *164*, 481–501. doi: 10.1016/j.gca.2015.02.040

Meert, J. G., Levashova, N. M., Bazhenov, M. L., & Landing, E. (2016). Rapid changes of magnetic Field polarity in the late Ediacaran: Linking the Cambrian evolutionary radiation and increased UV-B radiation. *Gondwana Research*, *34*, 149–157. doi: 10.1016/j.gr.2016.01.001

Meert, J. G., Pivarunas, A. F., Evans, D. A., Pisarevsky, S. A., Pesonen, L. J., Li, Z. X., ... Salminen, J. M. (2020). The magnificent seven: A proposal for modest revision of the Van der Voo (1990) quality index. *Tectonophysics*, *790*, 228549. doi: 10.1016/j.tecto.2020.228549

Meng, J., Coe, R. S., Wang, C., Gilder, S. A., Zhao, X., Liu, H., ... Li, S. (2017). Reduced convergence within the Tibetan Plateau by 26 Ma? *Geophysical Research Letters*, *44*(13), 6624–6632. doi: 10.1002/2017GL074219

Meng, J., Gilder, S. A., Li, Y., Chen, Y., Zhang, C., Zhou, Z., ... Wang, C. (2022). Remagnetization age and mechanism of Cretaceous sediments in relation to dyke intrusion, Hainan Island: Tectonic implications for South China and the Red River Fault. *Journal of Geophysical Research: Solid Earth*, *127*(1), 1–19. doi: 10.1029/2021JB023474

Niu, J., Li, Z. X., & Zhu, W. (2016). Palaeomagnetism and geochronology of mid-Neoproterozoic Yanbian dykes, South China: Implications for a c. 820-800 Ma true polar wander event and the reconstruction of Rodinia. *Geological Society Special Publication*, *424*(1), 192–211. doi: 10.1144/SP424.11

Ogg, J. G. (2012). Geomagnetic Polarity Time Scale. *The Geologic Time Scale 2012*, *1-2*, 85–113. doi: 10.1016/B978-0-444-59425-9.00005-6

Opdyke, N. D., & DiVenere, V. J. (2004). The magnetic polarity stratigraphy of the Mauch Chunk Formation, Pennsylvania. *Proceedings of the National Academy of Sciences*, *101*(37), 13423–13427. doi: 10.1073/pnas.0403786101

O'Reilly, W. (1984). Magnetic properties of other mineral systems. In *Rock and mineral magnetism* (pp. 172–193). Boston: Springer US. doi: 10.1007/978-1-4684-8468-7_8

Özdemir, Ö., & Dunlop, D. J. (2002). Thermoremanence and stable memory of single-domain hematites. *Geophysical Research Letters*, *29*(18), 10–13. doi: 10.1029/2002GL015597

Özdemir, Ö., & Dunlop, D. J. (2005). Thermoremanent magnetization of multidomain hematite. *Journal of Geophysical Research*, *110*(B09104), 1–8. doi: 10.1029/2005JB003820

Özdemir, Ö., & Dunlop, D. J. (2014). Hysteresis and coercivity of hematite. *Journal of Geophysical Research: Solid Earth*, *119*(4), 2582–2594. doi: 10.1002/2013JB010739

Özdemir, Ö., Dunlop, D. J., & Berquó, T. S. (2008). Morin transition in hematite: Size dependence and thermal hysteresis. *Geochemistry, Geophysics, Geosystems*, *9*(10). doi: 10.1029/2008GC002110

Park, Y., Swanson-Hysell, N. L., Xian, H., Zhang, S., Condon, D. J., Fu, H., & Macdonald, F. A. (2021). A Consistently High-Latitude South China From 820 to 780 Ma: Implications for Exclusion From Rodinia and the Feasibility of Large-Scale True Polar Wander. *Journal of Geophysical Research: Solid Earth*, *126*(6), 1–29. doi: 10.1029/2020JB021541

Parry, W. T., Chan, M. A., & Beitler, B. (2004). Chemical bleaching indicates episodes of fluid flow in deformation bands in sandstone. *American Association of Petroleum Geologists Bulletin*, *88*(2), 175–191. doi: 10.1306/09090303034

Raub, T. D., Kirschvink, J. L., & Evans, D. A. (2015). True Polar Wander: Linking Deep and Shallow Geodynamics to Hydro- and Biospheric Hypotheses. *Treatise on Geophysics: Second Edition*, *5*(1969), 511–530. doi: 10.1016/B978-0-444-53802-4.00108-1

Roberts, A. P., Cui, Y., & Verosub, K. L. (1995). Wasp-waisted hysteresis loops: Mineral magnetic characteristics and discrimination of components in mixed magnetic systems. *Journal of Geophysical Research*, *100*(B9), 17909–17924. doi: 10.1029/95jb00672

Roberts, N. M. (2013). The boring billion? - Lid tectonics, continental growth and environmental change associated with the Columbia supercontinent. *Geoscience Frontiers*, *4*(6), 681–691. doi: 10.1016/j.gsf.2013.05.004

Rochette, P., Mathé, P. E., Esteban, L., Rakoto, H., Bouchez, J. L., Liu, Q., & Torrent, J. (2005). Non-saturation of the defect moment of goethite and fine-grained hematite up to 57 Teslas. *Geophysical Research Letters*, *32*(22), 1–4. doi: 10.1029/2005GL024196

Saint-Bezar, B., Hebert, R. L., Aubourg, C., Robion, P., Swennen, R., & Frizon De Lamotte, D. (2002). Magnetic fabric and petrographic investigation of

hematite-bearing sandstones within ramp-related folds: Examples from the South Atlas Front (Morocco). *Journal of Structural Geology*, *24*(9), 1507–1520. doi: 10.1016/S0191-8141(01)00140-7

Schaltegger, U., Ovtcharova, M., Gaynor, S. P., Schoene, B., Wotzlaw, J. F., Davies, J. F., ... Chelle-Michou, C. (2021). Long-term repeatability and interlaboratory reproducibility of high-precision ID-TIMS U-Pb geochronology. *Journal of Analytical Atomic Spectrometry*, *36*(7), 1466–1477. doi: 10.1039/d1ja00116g

Schaltegger, U., Schmitt, A. K., & Horstwood, A. (2015). U-Th-Pb zircon geochronology by ID-TIMS, SIMS, and laser. *Chemical Geology*, *402*(8), 89–110.

Schmitz, B., Bergström, S. M., & Xiaofeng, W. (2010). The middle Darriwilian (Ordovician) δ13C excursion (MDICE) discovered in the Yangtze Platform succession in China: Implications of its first recorded occurrences outside Baltoscandia. *Journal of the Geological Society*, *167*(2), 249–259. doi: 10.1144/0016-76492009-080

Schoene, B., Crowley, J. L., Condon, D. J., Schmitz, M. D., & Bowring, S. A. (2006). Reassessing the uranium decay constants for geochronology using ID-TIMS U-Pb data. *Geochimica et Cosmochimica Acta*, *70*(2), 426–445. doi: 10.1016/j.gca.2005.09.007

Song, G., Wang, X., Shi, X., & Jiang, G. (2017). New U-Pb age constraints on the upper Banxi Group and synchrony of the Sturtian glaciation in South China. *Geoscience Frontiers*, *8*(5), 1161–1173. doi: 10.1016/j.gsf.2016.11.012

Sun, H.-Q., Huang, J.-Z., Guo, L.-Q., & Chen, J. (2012). Subdivision and isotopic age of Lengjiaxi Group in Hunan Province. *Geology and Mineral Resources of South China*, *28*(1), 20–26.

Swanson-Hysell, N. L., Fairchild, L. M., & Slotznick, S. P. (2019). Primary and Secondary Red Bed Magnetization Constrained by Fluvial Intraclasts. *Journal of Geophysical Research: Solid Earth*, *124*(5), 4276–4289. doi: 10.1029/2018JB017067

Swanson-Hysell, N. L., Maloof, A. C., Kirschvink, J. L., Evans, D. A., Halverson, G. P., & Hurtgen, M. T. (2012). Constraints on neoproterozoic paleogeography and paleozoic orogenesis from paleomagnetic records of the bitter springs formation, amadeus basin, central Australia. *American Journal of Science*, *312*(8), 817–884. doi: 10.2475/08.2012.01

Tan, X., Kodama, K. P., Gilder, S. A., Courtillot, V., & Cogné, J. P. (2007). Palaeomagnetic evidence and tectonic origin of clockwise rotations in the Yangtze fold belt, South China Block. *Geophysical Journal International*, *168*(1), 48–58. doi: 10.1111/j.1365-246X.2006.03195.x

Tauxe, L., & Kent, D. V. (2004). A simplified statistical model for the geomagnetic field and the detection of shallow bias in paleomagnetic inclinations: Was the ancient magnetic field dipolar? *Geophysical Monograph Series*, *145*, 101–115. doi: 10.1029/145GM08

Tauxe, L., Kent, D. V., & Opdyke, N. D. (1980). Magnetic components contributing to the NRM of Middle Siwalik red beds. *Earth and Planetary Science Letters*, *47*(2), 279–284. doi: 10.1016/0012-821X(80)90044-8

Tonti-Filippini, J. A. D., & Gilder, S. A. (2023). Vector unmixing of multicomponent palaeomagnetic data. *Geophysical Journal International*, *233*(3), 1632–1654. doi: 10.1093/gji/ggac505

Tonti-Filippini, J. A. D., Robert, B., Muller, E., Paul, A. N., Dellefant, F., Wack, M. R., ... Gilder, S. A. (2024). *Middle Neoproterozoic (Tonian) polar wander of South China: Paleomagnetism and ID-TIMS U-Pb geochronology of the Laoshanya Formation [Dataset].* Magnetics Information Consortium (MagIC). Retrieved from `earthref.org/MagIC/19728` doi: 10.7288/V4/MAGIC/19728

Torsvik, T. H. (2003). The Rodinia jigsaw puzzle. *Science*, *300*(5624), 1379–1381. doi: 10.1126/science.1083469

Torsvik, T. H., Domeier, M., & Cocks, L. R. M. (2021). Phanerozoic paleogeography and Pangea. In *Ancient supercontinents and the paleogeography of earth* (pp. 577–603).

Elsevier. doi: 10.1016/B978-0-12-818533-9.00003-5

Torsvik, T. H., Van der Voo, R., Preeden, U., Mac Niocaill, C., Steinberger, B., Doubrovine, P. V., ... Cocks, L. R. M. (2012). Phanerozoic Polar Wander, Palaeogeography and Dynamics. *Earth-Science Reviews*, *114*(3-4), 325–368. doi: 10.1016/j.earscirev.2012.06.007

Volk, M. W. R. (2016). *Influence of pressure, temperature and composition on magnetic recording in meteorites* (Doctoral dissertation, LMU Munich). doi: 10.5282/edoc.19824

Wack, M. R. (2023). Improved anisotropy of magnetic remanence results from vectorial readings using novel refinement method. *Geophysical Journal International*, *233*(2), 1113–1123. doi: 10.1093/gji/ggac500

Wack, M. R., & Gilder, S. A. (2012). The SushiBar: An automated system for paleomagnetic investigations. *Geochemistry, Geophysics, Geosystems*, *13*(12), 1–24. doi: 10.1029/2011GC003985

Walker, T. R., Larson, E. E., & Hoblitt, R. P. (1981). Nature and origin of hematite in the Moenkopi Formation (Triassic), Colorado Plateau: A contribution to the origin of magnetism in red beds. *Journal of Geophysical Research*, *86*(B1), 317–333. doi: 10.1029/JB086iB01p00317

Wang, H., Yuan, L., Wang, L., Zhou, Z., & An, J. (2016). Very Low-Grade Metamorphism of Clastic Rocks from the Meso-Neoproterozoic and the Paleozoic along the Profile Yueyang-Linxiang in Northeastern Hunan Province and Its Geological Implications. *Acta Geologica Sinica - English Edition*, *90*(5), 1743–1753. doi: 10.1111/1755-6724.12813

Wang, H., Zhou, Z., Wang, L., & Yuan, L. (2014). Anchimetamorphism and diagenesis of the Meso-Neoproterozoic and the Lower Paleozoic along profile Yangjiaping in North Hunan Province, China. *Yanshi Xuebao/Acta Petrologica Sinica*, *30*(10), 3013–3020.

Wang, J., Li, X., Duan, T., Liu, D., Song, B., Li, Z., & Gao, Y. (2003). Zircon SHRIMP U-Pb dating for the Cangshuipu volcanic rocks and its implications for the lower boundary age of the Nanhua strata in South China. *Chinese Science Bulletin*, *48*(16), 1663–1669. doi: 10.1360/03wd0168

Wang, J., & Li, Z. X. (2003). History of neoproterozoic rift basins in South China: Implications for Rodinia break-up. *Precambrian Research*, *122*(1-4), 141–158. doi: 10.1016/S0301-9268(02)00209-7

Wang, J., Zhou, X., Deng, Q., Fu, X., Duan, T., & Guo, X. (2015). Sedimentary successions and the onset of the Neoproterozoic Jiangnan sub-basin in the Nanhua rift, South China. *International Journal of Earth Sciences*, *104*(3), 521–539. doi: 10.1007/s00531-014-1107-5

Wang, Y., Fan, W., Zhao, G., Ji, S., & Peng, T. (2007). Zircon U-Pb geochronology of gneissic rocks in the Yunkai massif and its implications on the Caledonian event in the South China Block. *Gondwana Research*, *12*(4), 404–416. doi: 10.1016/j.gr.2006.10.003

Watson, G. S., & Enkin, R. J. (1993). The fold test in paleomagnetism as a parameter estimation problem. *Geophysical Research Letters*, *20*(19), 2135–2137. doi: 10.1029/93GL01901

Widmann, P., Davies, J. H., & Schaltegger, U. (2019). Calibrating chemical abrasion: Its effects on zircon crystal structure, chemical composition and U–Pb age. *Chemical Geology*, *511*, 1–10. doi: 10.1016/j.chemgeo.2019.02.026

Xian, H., Zhang, S., Li, H., Yang, T., & Wu, H. (2020). Geochronological and palaeomagnetic investigation of the Madiyi Formation, lower Banxi Group, South China: Implications for Rodinia reconstruction. *Precambrian Research*, *336*, 105494. doi: 10.1016/j.precamres.2019.105494

Xie, S.-k., Wang, Z.-j., Wang, J., & Zhuo, J.-w. (2012). LA-ICP-MS zircon U-Pb dating of the bentonites from the uppermost part of the Ordovician Wufeng Formation in the Haoping section, Taoyuan, Hunan. *Sedimentary and Tethyan Geology*, *4*, 597.

Xu, Y. J., Cawood, P. A., & Du, Y. S. (2016). Intraplate orogenesis in response to Gondwana assembly: Kwangsian Orogeny, South China. *American Journal of Science*, *316*(4), 329–362. doi: 10.2475/04.2016.02

Yan, D. P., Zhou, M. F., Song, H. L., Wang, X. W., & Malpas, J. (2003). Origin and tectonic significance of a Mesozoic multi-layer over-thrust system within Yangtze Block (South China). *Tectonophysics*, *361*(3-4), 239–254. doi: 10.1016/S0040-1951(02)00646-7

Yang, J., Luo, P., Ling, Y., Yang, S., Bai, D., Wei, F., ... Peng, N. (2021). Superimposed features and deformation mechanism of Early Mesozoic folds in the Sangzhi-Shimen area, northern Hunan. *Bulletin of Geological Science and Technology*, *40*(6), 43–54. doi: 10.19509/j.cnki.dzkq.2021.0605

Yang, S. X., & Blum, N. (1999). A fossil hydrothermal system or a source-bed in the Madiyi Formation near the Xiangxi Au-Sb-W deposit, NW Hunan, PR China? *Chemical Geology*, *155*(1-2), 151–169. doi: 10.1016/S0009-2541(98)00146-6

Yao, J., Cawood, P. A., Shu, L., & Zhao, G. (2019). Jiangnan Orogen, South China: A 970-820 Ma Rodinia margin accretionary belt. *Earth-Science Reviews*, *196*. doi: 10.1016/j.earscirev.2019.05.016

Yin, C., Gao, L., Xing, Y., Wang, Z., & Tang, F. (2004). Advances in the study on the Nanhua System of the Neoproterozoic and its stratotype in South China (in Chinese with English abstract). In *Professional papers of stratigraphy and palaeontology* (pp. 1–10). Beijing: Geological Publishing House.

Yin, C., Liu, D., Gao, L., Wang, Z., Xing, Y., Jian, P., & Shi, Y. (2003). Lower boundary age of the Nanhua System and the Gucheng glacial stage: Evidence from SHRIMP II dating. *Chinese Science Bulletin*, *48*(16), 1657–1662. doi: 10.1360/03wd0112

Zhang, H. (1998). Preliminary Proterozoic apparent polar wander paths for the South China Block and their tectonic implications. *Canadian Journal of Earth Sciences*, *35*(3), 302–320. doi: 10.1139/e97-117

Zhang, Q. R., & Piper, J. D. (1997). Palaeomagnetic study of Neoproterozoic glacial rocks of the Yangzi Block: Palaeolatitude and configuration of South China in the late Proterozoic Supercontinent. *Precambrian Research*, *85*(3-4), 173–199.

Zhang, S., Chang, L., Zhao, H., Ding, J., Xian, H., Li, H., ... Yang, T. (2021). The Precambrian drift history and paleogeography of the Chinese cratons. In *Ancient supercontinents and the paleogeography of earth* (pp. 333–376). Elsevier. doi: 10.1016/B978-0-12-818533-9.00005-9

Zhang, S., Jiang, G. Q., Dong, J., Han, Y. G., & Wu, H. C. (2008). New SHRIMP U-Pb age from the Wuqiangxi Formation of Banxi Group: Implications for rifting and stratigraphic erosion associated with the early Cryogenian (Sturtian) glaciation in South China. *Science in China, Series D: Earth Sciences*, *51*(11), 1537–1544. doi: 10.1007/s11430-008-0119-z

Zhang, S., Li, H., Jiang, G., Evans, D. A., Dong, J., Wu, H., ... Xiao, Q. (2015). New paleomagnetic results from the Ediacaran Doushantuo Formation in South China and their paleogeographic implications. *Precambrian Research*, *259*, 130–142. doi: 10.1016/j.precamres.2014.09.018

Zhang, X., Wang, Y., & Chen, X. (2000). Diagenesis and Porosity of the Cambrian-Ordovician Carbonate Shoal Facies at Yangjiaping, Shimen, Hunan. *Acta Geologica Sinica - English Edition*, *74*(1), 29–45. doi: 10.1111/j.1755-6724.2000.tb00429.x

Zhang, Y., Wang, Y., Zhang, Y., & Zhang, A. (2015). Neoproterozoic assembly of the Yangtze and Cathaysia blocks: Evidence from the Cangshuipu Group and associated rocks along the Central Jiangnan Orogen, South China. *Precambrian Research*, *269*, 18–30. doi: 10.1016/j.precamres.2015.08.003

Zhao, G., Wang, Y., Huang, B., Dong, Y., Li, S., Zhang, G., & Yu, S. (2018). Geological reconstructions of the East Asian blocks: From the breakup of Rodinia to the assembly of Pangea. *Earth-Science Reviews*, *186*(October), 262–286. doi: 10.1016/j.earscirev.2018.10.003

Zheng, B., Zhou, R., Mou, C., Wang, X., Xiao, Z., & Chen, Y. (2020). Nature of the Late Ordovician-Early Silurian Xiaohe section, Hunan-Hubei area, South China: implications for the Kwangsian Orogeny. *International Geology Review*, *62*(10), 1262–1272. doi: 10.1080/00206814.2019.1644541

Zijderveld, J. (1967). A.C. demagnetization of rocks: Analysis of results. In S. Runcorn, K. Creer, & D. Collinson (Eds.), *Methods in palaeomagnetism* (pp. 254–286). Amsterdam: Elsevier.

Additional references from supporting information

Bai, L., Zhu, R., Wu, H., Guo, B., & Lü, J. (1998). New Cambrian paleomagnetic pole for Yangtze Block. *Science in China, Series D: Earth Sciences*, *41*, 70–71. doi: 10.1360/yd1998-41-S2-66

Fang, W., Voo, R. V. D., & Liang, Q. (1990). Ordovician Paleomagnetism of Eastern Yunnan, China. *Geophysical Research Letters*, *17*(7), 953–956.

Flinn, D. (1962). On folding during three-dimensional progressive deformation. *Quarterly Journal of the Geological Society*, *118*(1-4), 385–428. doi: 10.1144/gsjgs.118.1.0385

Gao, L., Yang, Z., Han, Z., Tong, Y., Jing, X., & Zhang, S. H. (2018). Remagnetization of the Lower Ordovician Hongshiya Formation of the southwestern Yangtze Block. *Tectonophysics*, *738-739*, 83–91. doi: 10.1016/j.tecto.2018.05.017

Han, Z., Yang, Z., Tong, Y., & Jing, X. (2015). New paleomagnetic results from Late Ordovician rocks of the Yangtze Block, South China, and their paleogeographic implications. *Journal of Geophysical Research: Solid Earth*, *120*(7), 4759–4772. doi: 10.1002/2015JB012005

Huang, K., Opdyke, N. D., & Zhu, R. (2000). Further paleomagnetic results from the Silurian of the Yangtze Block and their implications. *Earth and Planetary Science Letters*, *175*(3-4), 191–202. doi: 10.1016/S0012-821X(99)00302-7

Jiang, X. S., Wang, J., Cui, X. Z., Zhuo, J. W., Xiong, G. Q., Lu, J. Z., & Liu, J. H. (2012). Zircon SHRIMP U-Pb geochronology of the Neoproterozoic Chengjiang Formation in central Yunnan Province (SW China) and its geological significance. *Science China Earth Sciences*, *55*(11), 1815–1826. doi: 10.1007/s11430-012-4530-0

Opdyke, N. D., Huang, K., Xu, G., Zhang, W., & Kent, D. (1987). Paleomagnetic results from the Silurian of the Yangtze paraplatform. *Tectonophysics*, *139*(1-2), 123–132. doi: 10.1016/0040-1951(87)90201-0

Wang, W., Zhou, M. F., Zhao, J. H., Pandit, M. K., Zheng, J. P., & Liu, Z. R. (2016). Neoproterozoic active continental margin in the southeastern Yangtze Block of South China: Evidence from the ca. 830–810 Ma sedimentary strata. *Sedimentary Geology*, *342*, 254–267. doi: 10.1016/j.sedgeo.2016.07.006

Yang, Z., Sun, Z., Yang, T., & Pei, J. (2004). A long connection (750-380 Ma) between South China and Australia: Paleomagnetic constraints. *Earth and Planetary Science Letters*, *220*(3-4), 423–434. doi: 10.1016/S0012-821X(04)00053-6

Zhang, S., Li, H., Zhang, X., Wu, H., Yang, T., Liu, Y., & Cao, Q. (2012). New Ordovician paleomagnetic results from South China Block and their paleogeographic implications. *The 34th IGC abstract*.